Texas A&M University
Mechanical Engineering Department
Turbomachinery Laboratory
Tribology Group

More on Metal Mesh Foil Bearings: Effect of Excitation Frequency on Dynamic Force Coefficients

Research Progress Report to the TAMU Turbomachinery Research Consortium

TRC– B&C-01-10

By

Luis San Andrés
Mast-Childs Tribology Professor
Principal Investigator

Thomas Abraham Chirathadam
Research Assistant

May 2010

Metal Mesh-Top Foil Bearings for Oil-Free Turbomachinery
TRC Project, TEES # 32513/1519 V2

EXECUTIVE SUMMARY

Metal mesh foil bearings (MMFBs), easy to construct and inexpensive, are a promising reliable bearing technology for oil-free microturbomachinery operating at high speeds and high temperatures. Research at TAMU has demonstrated the near friction-free operation of MMFBs operating at high speeds (60 krpm max.) and showing substantial energy dissipation (large damping) characteristics due to the multitude of micro slips within its metal mesh structure.

This report details further experimental work on a metal mesh foil bearing (MMFBs) towards determining its rotordynamic force coefficients from dynamic load tests. The test rig comprises of a turbocharger driven shaft and overhang journal onto which a MMFB is installed. A soft elastic support structure akin to a squirrel cage holds the test bearing, aiding to its accurate positioning relative to the rotating journal. Two orthogonally positioned electromagnetic shakers excite the test element via stingers. These shakers, 45° away from the vertical direction, hung from a hardy metal frame. The test MMFB comprises of a cartridge holding a Copper wire ring, 2.7 mm thick[1], and a top arcuate foil made of Inconel, 0.12 mm thick. The journal diameter and bearing length equal 38 mm. The constructed MMFB offers a compact sized bearing design in a space envelope similar to that of commercially available bump type foil bearings.

Initial impulse load measurements were conducted on the bearing and support cage alone to identify the soft structure stiffness and damping coefficients, as well as the effective bearing system mass. The identified structure stiffness and damping coefficients are relatively small when compared to the MMFB force coefficients.

A PC based DAQ system is customized to build the dynamic loads, sine-sweep in form; with specified amplitudes to ensure the bearing displacements (relative to the rotor) are within prescribed limits. Experiments were conducted with no journal rotation and with the journal spinning at 50 krpm (833 Hz) and with a static (pull) load of 22 N acting on the bearing.

Bearing motions (displacements and accelerations) result from the application of dynamic load vectors with excitation frequencies ranging from 250-400 Hz. The forces and bearing motions are recorded and later processed in the frequency domain. The identification procedure requires of (sets of) two independent load vectors to render four impedance coefficients, whose real and imaginary parts reveal 4 stiffness and 4 damping force coefficients, both parameters

[1] A prior bearing, with same mesh density or compactness (20%), had a thicker mesh (6.9 mm), see Refs. [1-3]

being frequency dependent. Multiple independent tests show the identified force coefficients are consistent, as per repeatability, for excitation frequencies lower than 350 Hz only.

Tests are conducted with an applied vertical pull load of 22 N, without journal rotation and with the journal spinning at 50 krpm (833 Hz). A discussion of the force coefficients follows over the range of frequencies [250-350 Hz] where the test data is most repeatable. In general, however, the current MMFB force coefficients are less frequency dependent than in prior measurements.

With no journal spinning, the force coefficients correspond to those of the bearing structure alone since the journal and bearing are in contact. The direct stiffnesses are relatively invariant (~0.4MN/m) with frequency while the damping coefficients decrease (600 Ns/m to 200 Ns/m), as expected. The cross coupled coefficients are nil.

Journal rotation induces airborne operation with a hydrodynamic gas film separating the rotor from its bearing. Hence, cross-coupled stiffnesses coefficients appear though with magnitudes lower than those of the direct stiffness coefficients. The principal stiffnesses (0.35 to 0.45 MN/m within 250-350 Hz) are similar in magnitude as those obtained without journal rotation suggesting the air film stiffness is quite high. Surprisingly, direct damping coefficients are nearly constant (~ 400 Ns/m), i.e. not decreasing as frequency grows.

The measurements evidence a test bearing system with lots of damping, overdamped in actuality. Analysis of the energy dissipation in the test MMFB reveals a material loss factor (γ) > 1.0. This loss factor is at least two fold that obtained with a similar size MMFB, but with a thinner metal mesh ring. The tested MMFB has a remarkable large damping ability!

Further testing produced failure of the bearing top foil without compromising the integrity of the test journal and drive turbocharger. Once the bearing is repaired with a new top foil, work will continue to perform measurements and parameter identification at other rotational speeds. Efforts to improve the robustness of the identification procedure will be in place. In addition, measurements with bump-type foil bearings (of exactly the same size) are forthcoming to provide a one to one comparison with the MMFB force coefficients.

Dr. Luis San Andrés proofread and edited five times an original draft by Thomas Chirathadam. Dr. San Andrés spent no less than 30 hours analyzing the test data, rewriting profusely all sections of this report.

TABLE OF CONTENTS

MORE ON METAL MESH FOIL BEARINGS: EFFECT OF EXCITATION FREQUENCY ON DYNAMIC FORCE COEFFICIENTS

LUIS SAN ANDRES, MAY 2010

LIST OF TABLES

LIST OF FIGURES

NOMENCLATURE

$a_{X(t)}$, $a_{Y(t)}$	Bearing accelerations, X and Y directions [m/s^2]
$\bar{A}_{X_{(\omega)}}$, $\bar{A}_{Y_{(\omega)}}$	DFT of X,Y bearing accelerations [m/s^2]
$\{C_{\alpha\beta}\}$ $\alpha\beta=X,Y$	Bearing damping coefficients [Ns/m]
$\{C_{S\beta}\}$ $\beta=X,Y$	Support structure damping coefficients [Ns/m]
D	Journal diameter [m]
D_{Bi} , D_{Bo}	Bearing cartridge inner and outer diameters [m]
D_{MMi} , D_{MMo}	Metal mesh ring inner and outer diameters [m]
E_V, E_M	Energy dissipated (viscous and hysteretic)[J]
$F(t)$	Sine sweep force function [V]
F_o	Force applied at the lowest test frequency [V]
ΔF	Rate of change of applied force in voltage [V]
F_X, F_Y	External excitation force [N]
$\bar{F}_{X(\omega)}, \bar{F}_{Y(\omega)}$	DFT of excitation forces [N]
$\{H_{\alpha\beta}\}$ $\alpha\beta=X,Y$	$K_{\alpha\beta}+j\,\omega\,C_{\alpha\beta}$. Bearing impedance coefficients [N/m], $j=\sqrt{-1}$
$\{K_{\alpha\beta}\}$ $\alpha\beta=X,Y$	Bearing stiffness coefficients [N/m]
$\{K_{S\beta}\}$ $\beta=X,Y$	Support structure stiffness coefficients [N/m]
L	Bearing axial length [m]
M	Bearing mass[kg]
$\{M_{\alpha\beta}\}$ $\alpha\beta=X,Y$	Inertia force coefficients [Ns/m]
$\{M_{S\beta}\}$ $\beta=X,Y$	Estimated test system masses [kg]
t	Time [s]
T	$2\pi/\omega$. Time period [s]
T_{tf}	Top foil thickness [m]
$x_{(t)}, y_{(t)}$	Bearing displacements relative to journal [m]
$X_{(t)}, Y_{(t)}$	Bearing absolute displacements along X, Y [m]
$\bar{x}_{(\omega)}, \bar{y}_{(\omega)}$	DFT of bearing X,Y displacements relative to journal [m]
γ	Metal mesh bearing loss factor [-]
ω	Excitation frequency [rad/s]
ω_o	Low frequency excitation [rad/s]

$\Delta\omega$	Rate of change in excitation frequency [rad/s]
Ω	Rotor speed [rad/s]
ζ	Damping ratio [-]

Matrices and Vectors

F	$\{F_X, F_Y\}^T$ Lateral reaction force vector [N]
H	**K** + iω **C**. Matrix of bearing impedance coefficients [N/m]
K,C,M	Matrices of stiffness, damping and inertia force coefficients
z	$\{x_{(t)}, y_{(t)}\}^T$. Bearing displacement vector, time domain [m]

Acronyms

DFT	Discrete Fourier Transform Operator
MMFB	Metal Mesh Foil Bearing
RBS	Rotor Bearing Systems
TC	Turbocharger

INTRODUCTION

Lubricated film bearings and seals in rotating mechanical systems play a fundamental role in their dynamic forced performance. A bearing reacts to rotor lateral motions with dynamic forces characterized by stiffness and damping coefficients. The rotordynamic (linear) force coefficients are a function of the bearing geometry and lubricant (gas or liquid), and operating conditions including rotor speed and applied load. Gas bearings and seals also show frequency dependent force coefficients because of the lubricant compressibility, in particular at high rotational speed and high frequency operation. Bearing direct stiffness and damping coefficients largely determine the placement of rotor bearing system (RBS) critical speeds and damping ratios; while cross-coupled stiffness coefficients, ensuing from hydrodynamic film shear from rotor spinning, can lead to loss of effective damping and the onset of rotordynamic instability, typically at fractional frequencies of rotor speed and coinciding with system natural frequencies.

Gas bearing lubricated rotor bearing systems are compact with less number of parts and more efficient because of their high temperature operation with minute power losses. Oil-free RBS are nearly maintenance free and offer long operating life. Gas foil bearings typically find application in moderate load systems like micro power generators, Air Cycle Machines (ACMs), cryogenic turbocompressors, and turbo expanders. A metal mesh foil bearing (MMFB) is a type of gas foil bearing that incorporates a thin metal mesh ring and a pre-formed smooth top foil within a bearing cartridge [1]. While mechanical energy dissipation in commercially available gas foils bearing (GFB), bump-type for instance, is primarily due to Coulomb dry-friction, MMFB offer larger energy dissipation due to material hysteresis as well as dry-friction.

OVERVIEW OF RESEARCH IN METAL MESH FOIL BEARINGS AT TAMU

Metal mesh foil bearings are a non proprietary bearing technology whose underspring support is made of commercial materials. Hence, their construction is simple and inexpensive. These are major advantages when compared to commercial bump-type foil bearings. San Andrés and students [1-3], with TRC support, spear head the technology development in MMFBs in a concerted effort to demonstrate their reliable high speed operation with large loads (per unit area), extremely low frictional losses, and unique rotordynamic force characteristics.

San Andrés *et al*. [1] report constructing the first prototype of a MMFB (L=D=28.00 mm) with a metal mesh ring made of 0.3 mm Copper wire and compactness of 20 %. With the test

bearing installed on a shaft with a slight preload, static load versus bearing deflection measurements display a cubic nonlinearity with large hysteresis indicating significant mechanical energy dissipation. Identified structural stiffness and viscous damping coefficients, similarly as in metal mesh dampers [4]; i.e., decrease with increasing motion amplitudes. However, with increasing frequency, while the viscous damping coefficient rapidly decreases, the stiffness grows. A structural loss factor (material damping), not viscous damping, best describes the mechanical energy dissipation of metal meshes. The experiments reveal a loss factor (γ) as high as 0.7, higher than that in bump-type foil bearings, for example. In Ref. [1], the authors noticed that the metal mesh ring undergoes significant sag or creep, resulting in the reduction of the magnitude of the force coefficients, upon operation and multiple dismantling and re-assembly processes.

Adequate load capacity, low frictional loss and reliable rotordynamic performance are important for the ready application of MMFBs into oil-free turbomachinery. San Andrés *et al.* [5] demonstrate the readiness of the novel bearing technology by measuring the MMFB break-away torque, rotor lift off and touchdown speeds during multiple start up and shutdown tests. Further, Ref. [2] extends the work reporting measured bearing load capacity and drag torque for rotor speeds to 60 krpm. During airborne operation, i.e., with a gas film separating the rotating journal from the bearing, the friction coefficient is orders of magnitude smaller than that during dry-friction operation at start up (and shut down) where rubbing contact prevails. The tests also demonstrated that a solid lubricant (coating) reduces the friction while in contact operation.

San Andrés and Chirathadam [3] employ unidirectional impact load tests to identify the direct and cross-coupled rotor dynamic force coefficients of a lightly loaded MMFB, floating on a test journal spinning at 50 krpm (833 Hz). A near centered operation is assumed thus leading to K_{XX}=K_{YY} and K_{XY}= -K_{YX}, for example. The test bearing force coefficients obtained with no journal rotation and with rotor spinning at 50 krpm (833 Hz) are similar in magnitude and trend over the excitation frequency range [10-200 Hz]. The results show the minute hydrodynamic gas film generated while the bearing is airborne does not affect significantly the bearing structural force coefficients. Bearing motions, recorded during rotor speed coast down tests, are complex in character with distinctive subsynchronous whirl frequencies of large amplitude. The subsynchronous whirl motions may be due to the MMFB stiffness hardening characteristics.

The report presents more rotordynamic measurements conducted with a new bearing whose metal mesh is just ~ 2.7 mm. The bearing is compact in size and robust in construction, still maintaining the same mesh density as the first prototype MMFB [1-3].

A REVIEW OF EXPERIMENTAL FOIL BEARING FORCE COEFFICIENTS

Experiments towards the identification of bearing force coefficients are important not just to verify performance of the mechanical element but also to benchmark predictive tools, hence aiding in the bearing design process and providing confidence in the use of the test element in actual rotor bearing systems (RBS). Often predictive tools are inaccurate or not yet mature enough[2], thus the need to perform experiments towards characterization of the bearing dynamic performance.

Bearing rotordynamic force coefficients are, by definition, changes in reaction forces due to small amplitude motions about an equilibrium position. The typical linear model for a bearing or seal is

$$\begin{Bmatrix} F_X \\ F_Y \end{Bmatrix} = -\begin{bmatrix} K_{XX} & K_{XY} \\ K_{YX} & K_{YY} \end{bmatrix} \begin{Bmatrix} x \\ y \end{Bmatrix} - \begin{bmatrix} C_{XX} & C_{XY} \\ C_{YX} & C_{YY} \end{bmatrix} \begin{Bmatrix} \dot{x} \\ \dot{y} \end{Bmatrix} - \begin{bmatrix} M_{XX} & M_{XY} \\ M_{YX} & M_{YY} \end{bmatrix} \begin{Bmatrix} \ddot{x} \\ \ddot{y} \end{Bmatrix} \tag{1a}$$

$$\mathbf{F} = -\mathbf{K}\,\mathbf{z} - \mathbf{C}\,\dot{\mathbf{z}} - \mathbf{M}\,\ddot{\mathbf{z}} \tag{1b}$$

where $\mathbf{F}=\{F_X,\ F_Y\}^T$ and $\mathbf{z}=\{x_{(t)}\ ,y_{(t)}\}^T$ are vectors of lateral reaction forces and displacements, respectively. The matrices **K, C, M** contain the stiffness, damping and inertia force coefficients, respectively. Stiffnesses represent the ratio of force to displacements, while damping coefficients denote changes in force due to variations in velocity, etc. Inertia force coefficients ($M_{\alpha\beta}$), until recently ignored, are relevant in dense fluids bearings and seals operating at high speeds and with large pressure differentials.

Identification of bearing force coefficients requires of external forces acting on the test element and the measurement of ensuing bearing dynamic displacements. Tiwari [6] reviews the most popular test techniques and analysis methods to identify linearized force coefficients in fluid film bearings. The methods include time and frequency domain procedures, while experimentation focuses on the types of dynamic load excitation most efficient for a particular

[2] The assertion is particularly true in foil bearings and many types of seals with complicated surface textures.

procedure. The review also includes physics based mathematical modeling with governing equations of the test bearing element or rotor-bearing system, parameter extraction algorithms, and uncertainty in the estimates. The classification of identification techniques is based on the method used to excite the test element or system: short duration (impacts and shock loads), periodic load excitation, fixed or sine-sweep and including imbalance induced forces, and random load excitation techniques [7]

In general, bearing force coefficients are frequency independent; the physical **K-C** model being more than adequate to represent bearing dynamic reaction forces. However, fluid compressibility leads to bearing stiffnesses that grow with excitation frequency while the damping decreases dramatically [8]. Hence, $\mathbf{K}=\mathbf{K}_{(\omega)}$ and $\mathbf{C}=\mathbf{C}_{(\omega)}$ are to be expected. Incidentally, mechanically complex bearings such as tilting pad bearings also show frequency dependent force coefficients, even when lubricated with a mineral oil (incompressible fluid). The frequency dependency is due to the complicated series interaction of the fluid film with the pads, undergoing translation and tilting rotation. Recently, Rodriguez and Childs [9] demonstrate that a **K-C-M** model represents well the dynamic force characteristics of tilting pad bearings.

Note also, from Eq. (1), that the damping coefficients are modeled as of *viscous* type, i.e. dissipation forces reacting to changes in velocity only. Recall that foil bearings have a distinctive mechanical energy dissipation mechanism due to dry-friction sliding between the top foil and the underlying bump strip layers and between the bump strips and the bearing ID. Similarly, in metal mesh bearings, damping arises from countless micro sliding actions amongst the wires within a compact mesh. Both actions are best represented as material or hysteretic damping with a loss factor (γ), empirically obtained. Hence, an equivalent viscous damping coefficient, $C \sim \gamma K/\omega$, is inversely proportional to the frequency (ω) of the motions[3]. Thus, in foil bearings (and metal mesh bearings too) the proper characterization of dissipation forces is particularly important. Often incorrect conclusions are drawn, for example that foil bearings have very large (viscous) damping coefficients as determined from experiments at (too) low excitation frequencies [10]; $C \to \infty \text{ as } \omega \to 0$ is not physically possible, better pointing out to a severe limitation of the viscous damping model.

There are only a handful of archival papers reporting experimental force coefficients for gas foil bearings, bump-type in particular. Metal mesh foil bearings are still a novelty. Prior art

abounds on the experimental identification and prediction of foil bearing structural stiffness and viscous damping coefficients, see Ref. [11] for an exhaustive review of past works. Structural force coefficients represent the mechanical parameters of the underspring structure (bump strip layers) and readily obtained in simple test rig configurations without rotor spinning**;** i.e. without the generation of the hydrodynamic gas film separating the journal from its top foil.

Howard [12] and Howard *et al.* [13] describe a test rig for measurement of load capacity and torque in gas foil bearings operating at high temperature (max. 538 °C). A bearing stiffness follows from load perturbations ensuing small bearing displacements while conducting the static load capacity measurements. The foil bearing stiffness drops, by a factor of two, as the operating temperature increases from ambient to 538 °C as the foil underspring material loses strength with increasing temperature. In general, the single[3] GFB stiffness increases with increasing applied loads, but decreases with increasing rotor speeds (30 krpm). Cross-coupled effects are thoroughly ignored. Later, Howard *et al.* [14] deliver impulse loads on the test foil bearing and record the ensuing bearing motion that decays as time elapses. Damping follows from the rate of peak amplitudes decay, i.e., estimation of log-decrement. At high temperature (538 °C) and for a low impact load (11.2 N), the viscous damping mechanism is dominant with little dry friction losses. However, larger impact loads excite large bearing motions and enable more energy dissipation from dry-friction damping, thus leading to a higher equivalent viscous damping coefficient; i.e. a quicker motion decay.

Lee *et al*. [15] are first to report a full set of stiffness (**K**) and damping (**C**) coefficients for a test GFB (L=D= 38.1mm) from measurements of impact loads and ensuing bearing displacements. The test bearing floats atop a rotor spinning to a top speed of 30 krpm and under a static load of 50 N. The identified **K** and **C** are regarded as frequency independent. Transfer functions from the impact loads show a test system with significant cross coupling of hydrodynamic type, underdamped (ζ~8 %–6 %) with a natural frequency at 80 Hz. The test bearing direct and cross coupled stiffnesses are nearly constant with increasing rotor speed; while the direct and cross-coupled damping coefficients decrease in magnitude. The test force coefficients show peculiar drops at the lowest speed (10 krpm). Cross-coupled stiffnesses are ~ 1/3 of the direct stiffnesses, while cross-damping force coefficients are relatively small when

[3] The parameter derived from single input (force)-single output(displacement)

compared to the direct damping force coefficients. Predicted bearing direct stiffnesses, derived from a model coupling the foil underspring structure to the gas film, do not agree well with the experimental force coefficients. The paper does not provide enough information on the bearing tested (geometry, materials, etc) to attempt comparisons with other available predictive tools.

Kim [16] compared measured imbalance responses obtained in a rigid rotor supported on 2nd generation GFBs (D=L=38.1mm), for cylindrical and preloaded with shims bearing configurations, with calculated rotordynamic responses using predicted foil bearing force coefficients. The measured rotor motion data served to identify effective (synchronous speed) GFB reduced stiffness and damping coefficients. The good agreement of the measured imbalance responses to the predicted ones based on linearized GFB force coefficients validates the predictive computational tool.

Recently, Conlon *et al.* [17] are the first to present GFB force coefficients over a range of excitation frequencies (to 300 Hz) and three rotor speeds (0, 15, 20 and 25 krpm). The test rig, similar in conception to the original rig of Glieneke [18] and constructed nearly identical to the rig of Childs and Hale [19], employs a floating bearing mounted on a rigid rotating shaft (max. speed of 30 krpm) that is supported on stiff ball bearings. A pair of shakers, orthogonally mounted, delivers loads onto the test element (L=D=70 mm). A frequency domain identification method, using power spectral density functions [20] to reduce data scattering, leads to an impedance matrix from which bearing stiffness and damping coefficients are extracted for frequencies. The test GFB shows both stiffness and damping coefficients are strong functions of the motion amplitude, excitation frequency and applied static load (max. 400 N). Rotor speed; albeit not its magnitude, does reduce the test element stiffness and damping coefficients, both decreasing dramatically with excitation frequency. Notorious dips in the direct stiffnesses are left unexplained. As expected, the bearing stiffness and damping coefficients increase mildly with increasing static load; again showing conspicuous dips at a frequency of 200 Hz.

The present work details a newly constructed test rig for identification of the rotordynamic force coefficients of small size gas bearings from measurements of shaker induced loads and bearing displacements and accelerations. The test metal mesh bearing, similar in size to commercial foil bearings, slides atop a journal that is driven by a commercial turbocharger air turbine. Measurements are conducted at a rotational speed of 50 krpm (833 Hz) with sine-sweep

dynamic loads with frequencies ranging from 250 Hz o 450 Hz. The report details the parameter identification procedure and presents the four stiffness and four damping coefficients versus excitation frequency. Comparisons with force coefficients obtained in experiments without journal rotation and under the same static load (22 N) evidence the effect of the gas film on the test bearing dynamic forced response.

TEST BEARING AND EXPERIMENTAL FACILITY

TEST METAL MESH FOIL BEARING

Figure 1 illustrates a cut view of a MMFB showing its components and relevant dimensions and Figure 2 pictures the test MMFB mounted on its journal. Table 1 lists the dimensions and specifications for the test bearing. The MMFB consists of a stainless steel bearing cartridge, a 20% dense copper mesh ring ~2.7 mm thick, and a smooth pre-formed(hot rolled) Inconel top foil,[4] 0.120 mm in thickness. One end of the top foil is inserted into a slot in the bearing cartridge, as shown in Figure 1. The slot[5] is angled in the direction of rotor spin. During bearing airborne operation, this arrangement prevents the top foil from spinning inside the bearing.

The metal mesh ring is manufactured by compressing a weave of thin copper wires into a flat strip. The strip is later folded and inserted into the bearing cartridge to take its arcuate shape. The mesh density, or compactness, is determined as the ratio of the ring mass to its volume times copper material density. The dimensions of the compressed strip of metal mesh are chosen such that it does not cover the slot in the bearing cartridge. Note that the metal mesh ring thickness[6] (2.7 mm) is about five times the height of a bump foil strip, when compared to a foil bearing available in the laboratory [12]. The top foil inner surface is spray coated with a thin layer

[4] Top foil donated by KIST, South Korea.
[5] The entire bearing was made in house and at a minimal cost. The slot has a width larger than that required to hold the top foil. A precisely dimensioned slot would require of a more complicated manufacturing. Presently, the loosely held top foil does not hinder the normal operation of the bearing. However, a commercial application would require of a narrow slot into which the top foil can be press fitted and locked in place.
[6] An earlier similar size MMFB had a thicker mesh (6.9 mm), Refs. [1-3]. The new bearing, with a thinner mesh thickness intends to replicate commercial foil bearing configurations. The thin metal mesh ring offers a compact sized bearing design in a space envelope similar to that of commercial bump type foil bearings. To manufacture the metal mesh ring, metal mesh strips are stacked up vertically and compressed under ~ 30 tons load to reach the desired density of 20% (compactness). The compressed flat metal mesh strip is then curved and inserted into the bearing cartridge, along with the top foil, to complete the construction of the MMFB.

(<5μm) of MoS_2 to reduce friction between the journal and top foil surface during rotor start up and shut down conditions. The application and curing process are at room temperature.

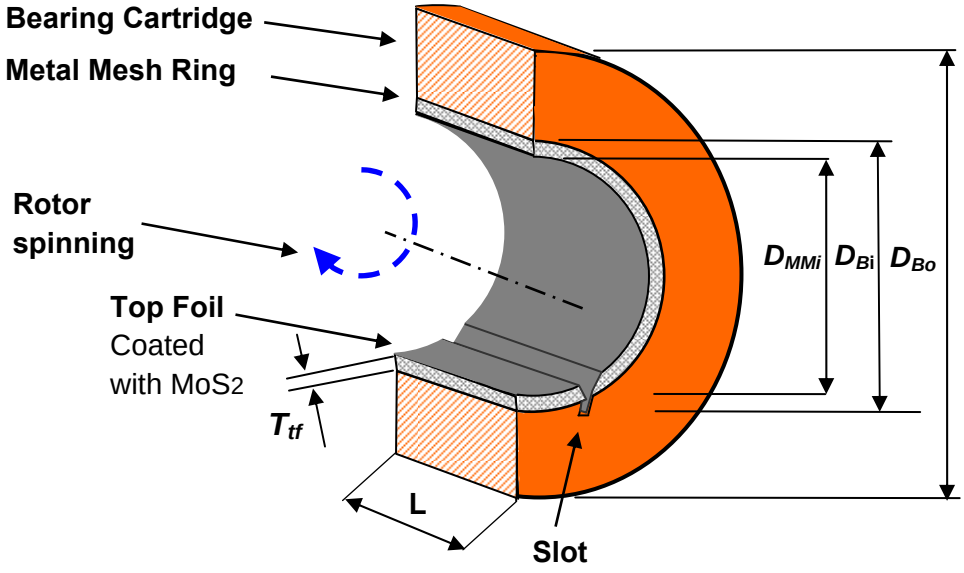

Fig. 1 Schematic cut view of a metal mesh foil bearing

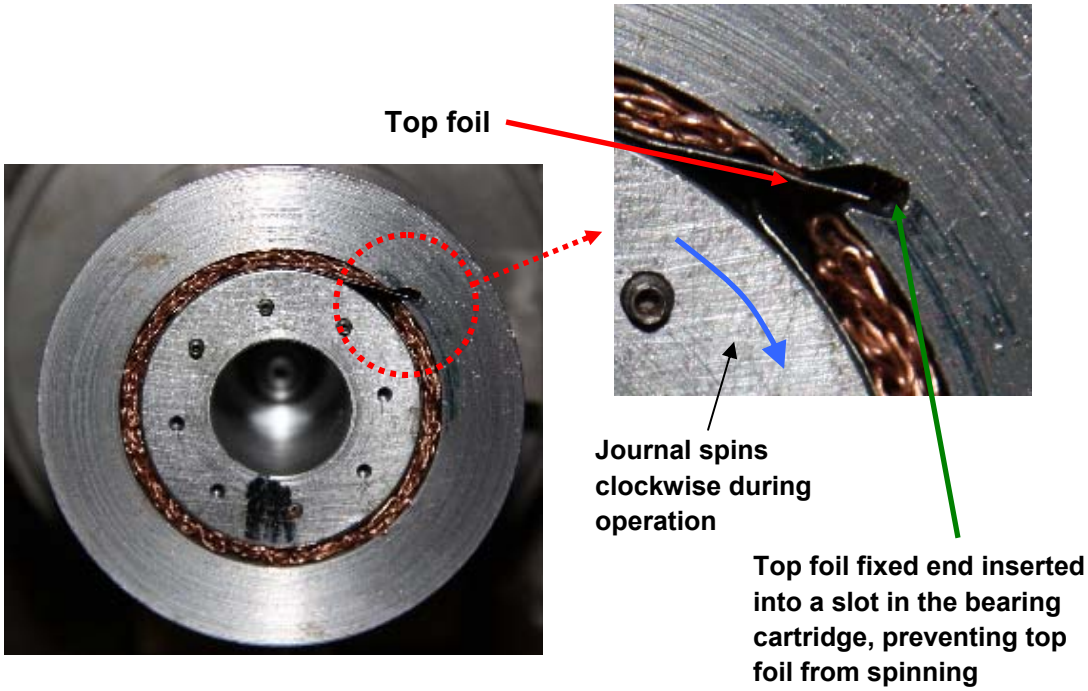

Fig. 2 Photograph of the MMFB mounted on the test journal. Inset shows a slot in the bearing cartridge for affixing the top foil

Table 1. MMFB nominal dimensions and material specifications

Parameter name and physical dimension	Magnitude
Bearing cartridge outer diameter, D_{Bo} (mm)	63.47 ± 0.02
Bearing cartridge inner diameter, D_{Bi} (mm)	41.75 ± 0.02
Bearing axial length, L (mm)	38.00 ± 0.02
Copper mesh outer diameter, D_{MMo} (mm)	41.75 ± 0.02
mesh inner diameter, D_{MMi} (mm)	36.35 ± 0.02
Copper mesh mass (g)	21.5
mesh density (%)	20
Copper mesh thickness (mm)	**2.70**
Inconel Top foil thickness (mm), T_{tf}	**0.12**
Wire diameter (mm)	0.30
Bearing mass (cartridge + mesh + foil +sensors), M (kg)	0.590

Uncertainty in mass measurement = ±0.0001 kg

TEST RIG DESCRIPTION

Figures 3 and 4 depict the test rig constructed for measurement of air gas bearing performance and identification of rotordynamic force coefficients. The photographs show the test MMFB, electromagnetic shakers (max. load 100 N), turbocharger (TC), and sensors to record relative bearing displacements, absolute bearing accelerations and shaker forces. The shakers are softly mounted from a rigid frame. A metal plate shield encloses the entire test setup thus ensuring operator safety. Note that the coordinate system (X-Y) is right handed with respect to the journal rotation.

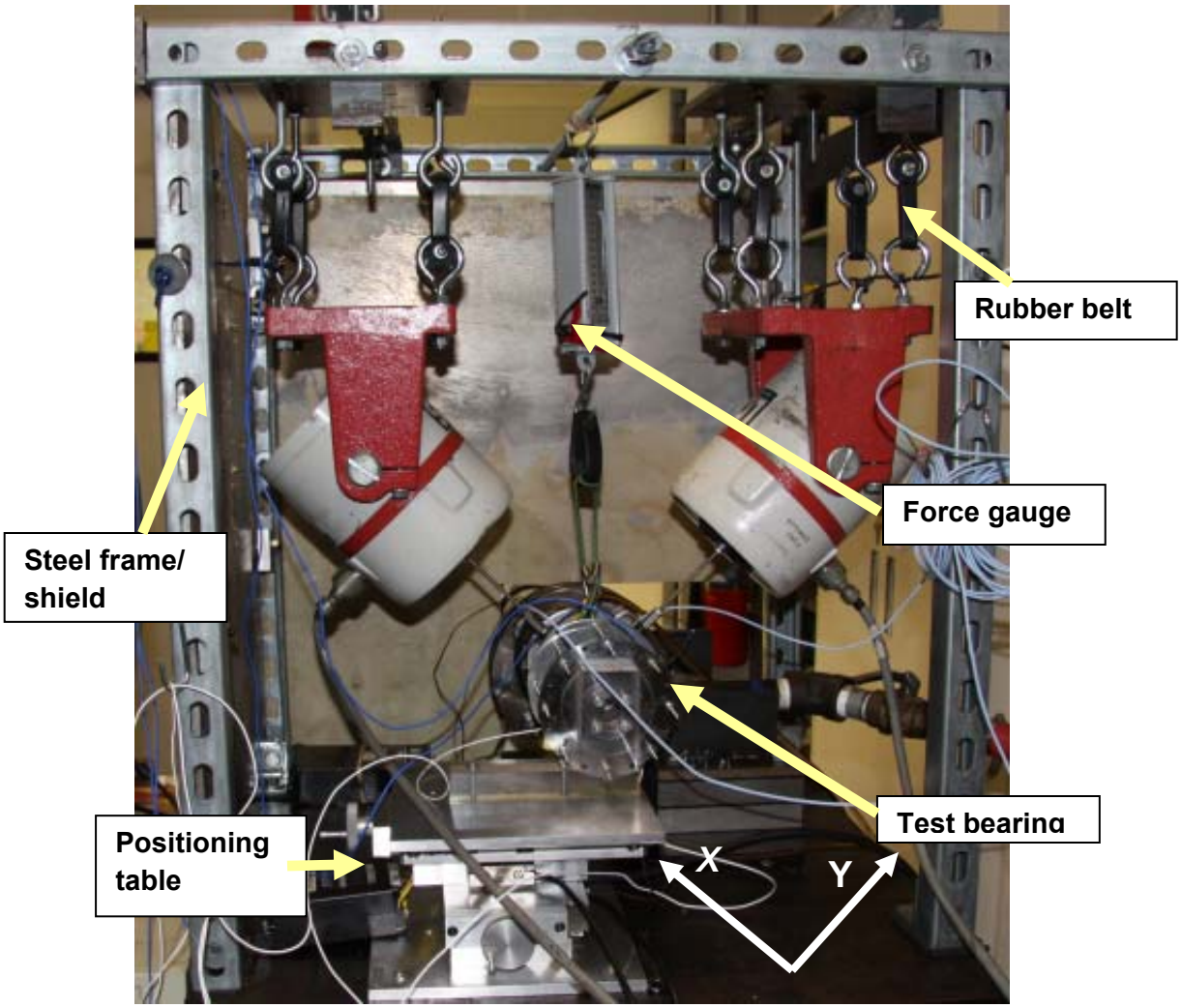

Fig. 3 Photograph of gas bearing test rig for dynamic load excitations

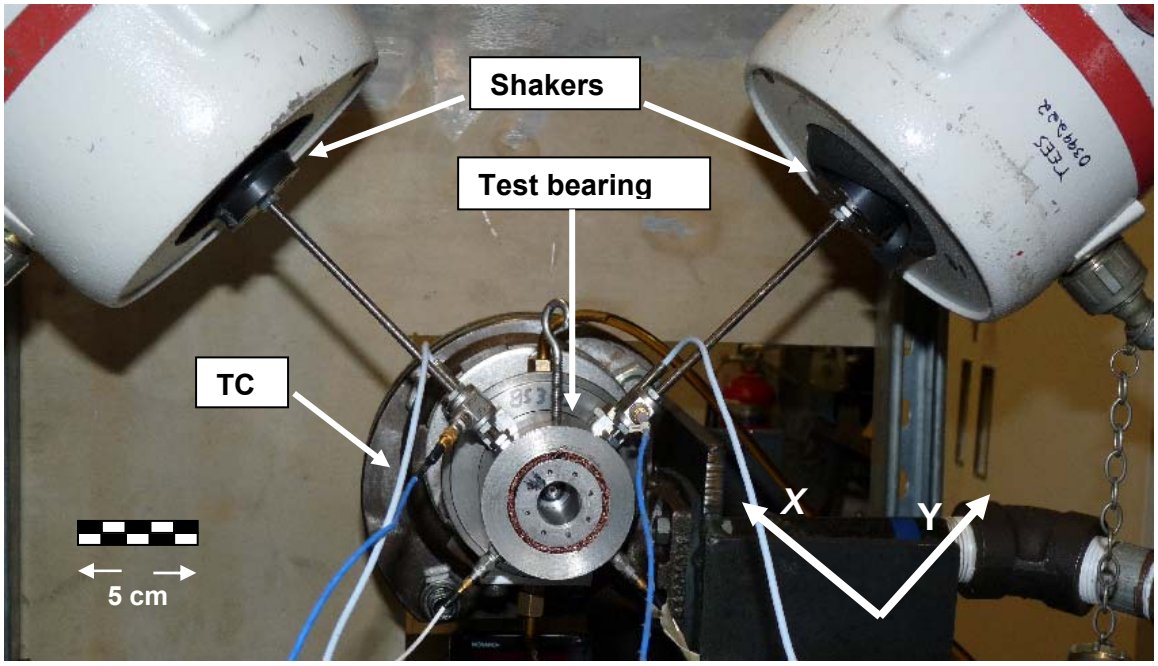

Fig. 4 Close-up view of metal mesh foil bearing and connections to shakers for dynamic load excitation

Figure 5 shows a schematic view of a ball bearing supported turbocharger (TC), with the compressor and its casing removed, driving a shaft stub onto which a hollow journal is mounted. The MMFB slides atop the journal of diameter D=38.00 mm and length 55.00 mm. The journal is initially coated with a thin layer (16 μm) of Permalon®, which however did not last long enough[7]. A squirrel-like cage supports the bearing with a low radial stiffness but high angular stiffness, thus reducing misalignment[8] with respect to the rotor during dynamic loading. The cage stiffness is so soft (~ 20 kN/m) that it does not affect significantly the dynamic load measurements.

[7] This coating, applied and cured at room temperature, is very soft. It only survived the very few initial tests with rotor spinning.

[8] Bearing force coefficients are derived from radial (lateral) forces and ensuing bearing displacements along two orthogonal directions. Accurate and reliable identification of force coefficient requires the test element not to displace axially, or worse yet not pitching (or yawing) with respect to the rotor spinning axis. Hence, it is common, as in Ref. [19], to implement external constraints to bearing rotations with pairs of taut cables, for example. These constraints, soft or very flexible along the radial direction, have a high rotational stiffnesses reducing pitch or yaw of the test element when excited.

The squirrel cage is affixed to a positioning table, turn knob controlled, that can displace horizontally. This feature aids in the easy removal and remounting of the test bearing into the journal. Two eddy current sensors affixed to the bearing cartridge record the displacement of the bearing with respect to the rotating journal. Two accelerometers affixed on the bearing cartridge, at its midspan, record the absolute acceleration of the bearing along two orthogonal directions. Two electromagnetic shakers apply dynamic loads on the bearing, via stingers and force sensors, the latter records the excitation load acting on the bearing.

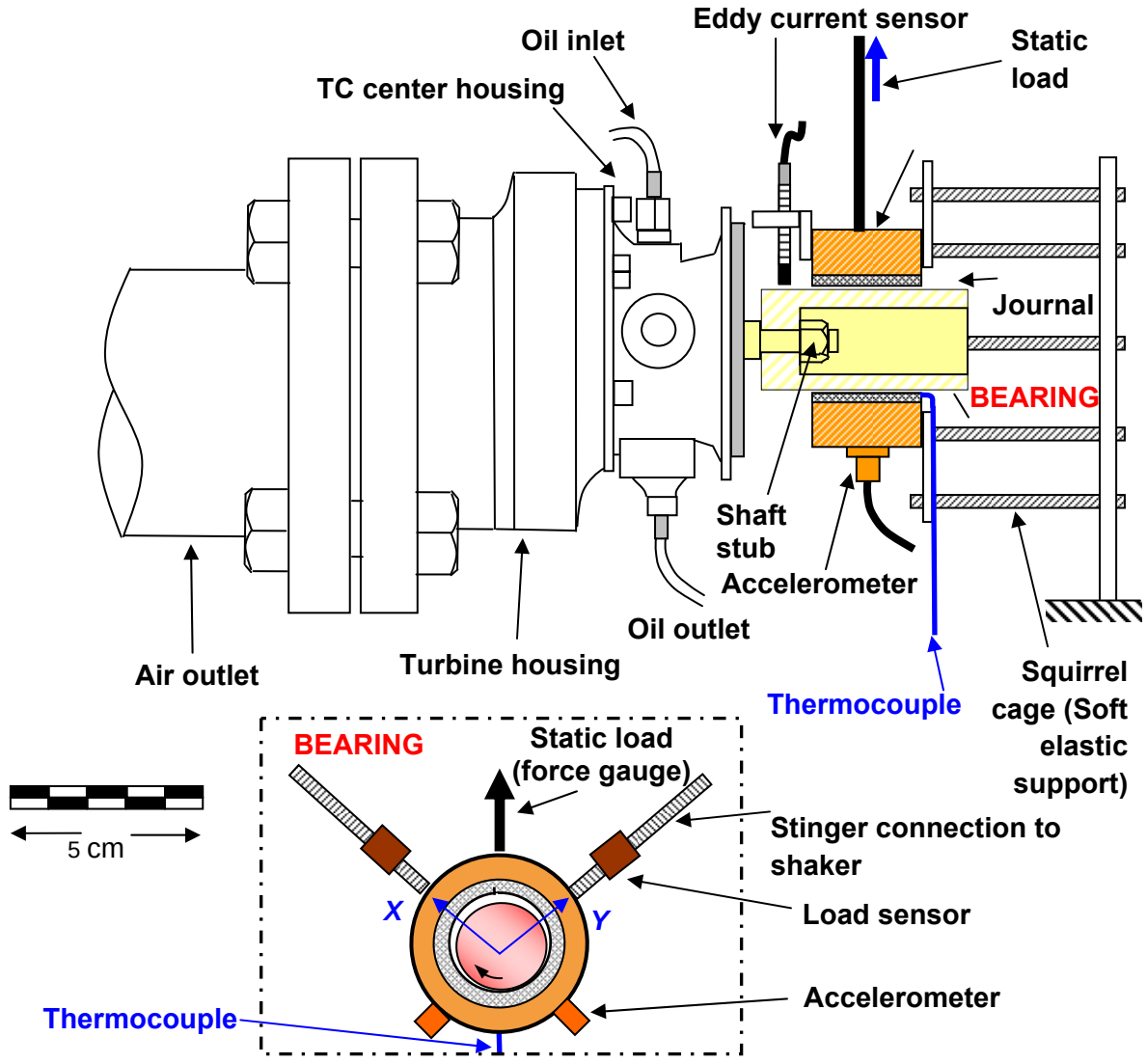

Fig. 5 Schematic view of MMFB mounted on shaft of turbocharger drive system. Inset shows two stingers for application of dynamic loads along two orthogonal directions

Static loads, measured with a force gauge, are applied in the vertically upward direction using strings tied onto a hook threaded in the bearing OD. An infrared tachometer records the turbine tip speed (± 0.0015% accuracy). The tachometer is located in the outlet air discharge pipe of the TC. A K-type thermocouple affixed at the outer end of the bearing measures the top foil temperature (± 0.5°C). The thermocouple is located opposite (180 degree away) to the static load, i.e., near the minimum film thickness position.

ESTIMATION OF STRUCTURAL PARAMETERS OF BEARING SUPPORT STRUCTURE

A soft elastic structure (squirrel cage), comprising of 8 thin steel rods, arranged in a circular pattern, holds the test bearing. In order to accurately determine the bearing force coefficients, the support structure stiffness and damping must be determined prior to bearing parameter identification. Note that the bearing is an overhung mass at the end of the squirrel cage. Figure 6 depicts typical impact loads (F_X, F_Y) delivered along two orthogonal directions, X and Y, on the test bearing. Refer to Fig. 4 for the orientation of the coordinates X and Y.

The figure also depicts the ensuing bearing accelerations (a_X, a_Y) versus time. In these measurements the bearing was not yet mounted on its journal and the shaker stingers were also not connected to the bearing cartridge.

Figure 7 shows average accelerations in the frequency domain. The data reveals a lightly damped system (ζ~0.037) with a fundamental elastic natural frequency at ~ 25 Hz. As expected, there is no structural cross-coupling.

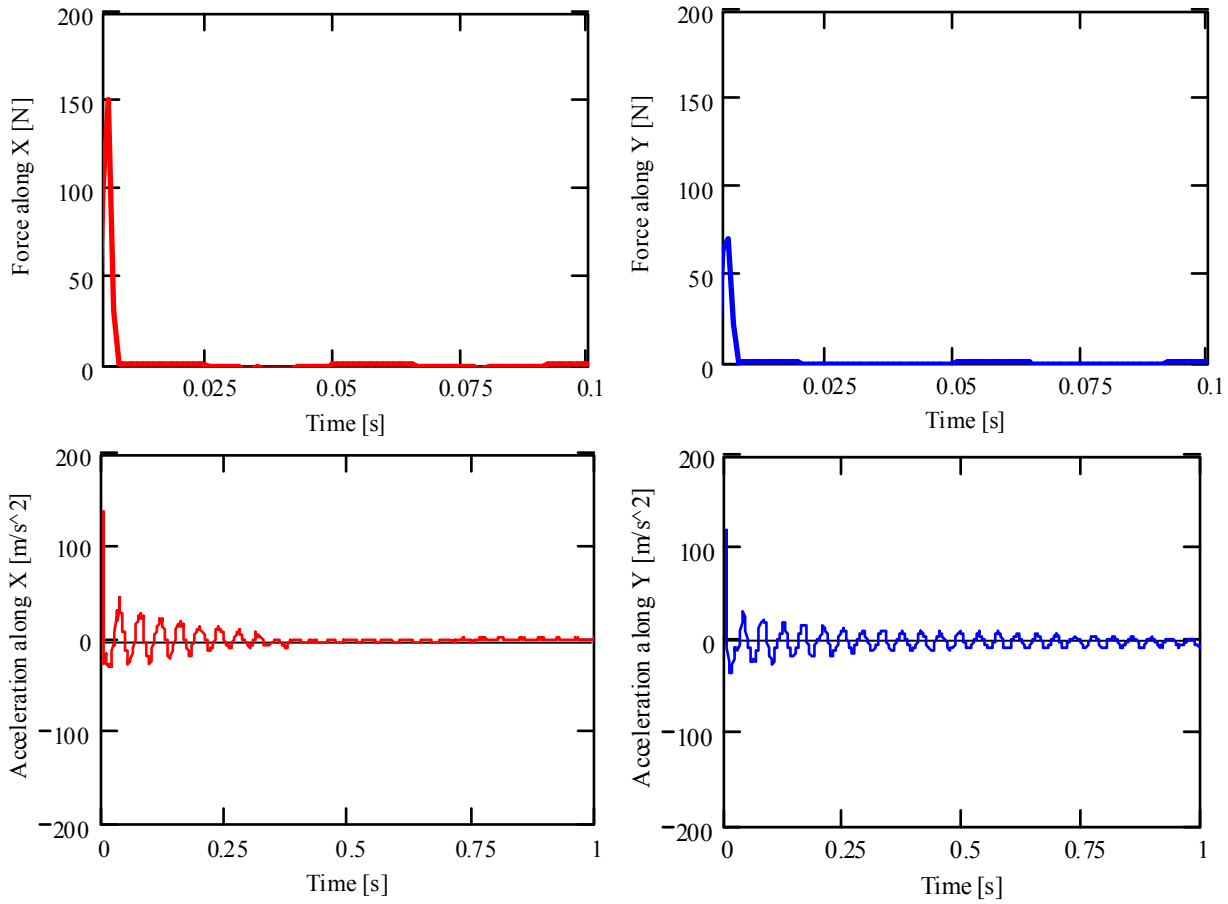

Fig. 6 Impact loads and recorded bearing accelerations, *X* and *Y* directions, versus time. No shaft rotation and no contact with journal

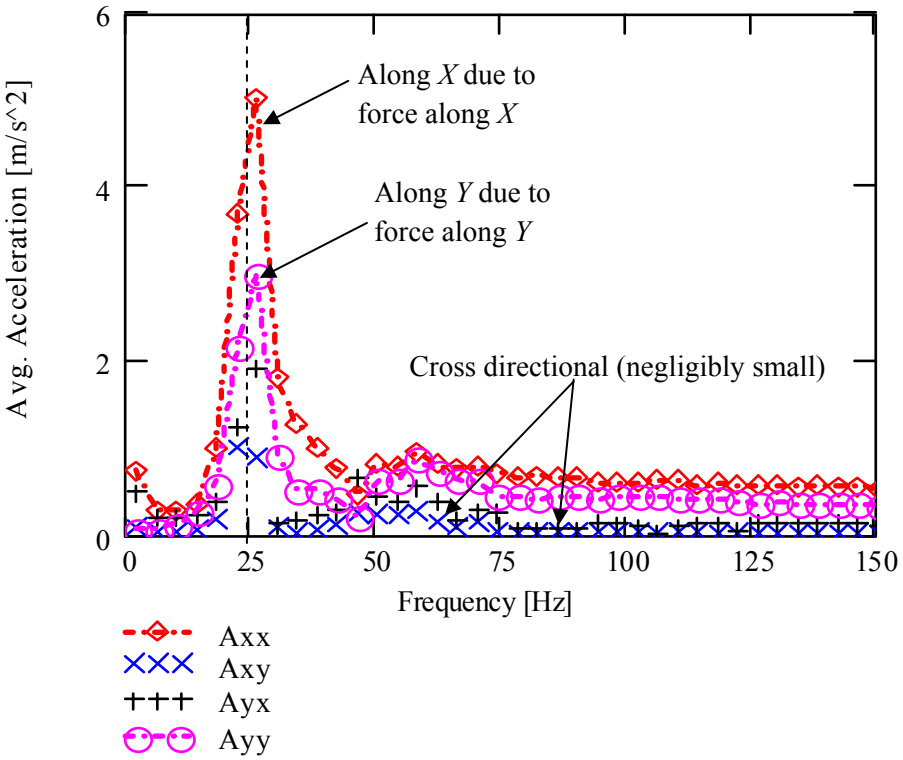

Fig. 7 *DFT* of (four averaged) accelerations along *X* and *Y* directions due to impact loads on bearing and elastic support structure

Since there is little structural cross-coupling, the squirrel cage and bearing behave as a single DOF mechanical system with mass M_S, stiffness K_S and viscous damping C_S coefficients along each direction (X,Y). From measurements of the acceleration and impact load, the parameters are extracted from a nonlinear curve fit of the recorded accelerance function to the physical model equation; for instance along X,

$$\left\| \left[\frac{a_{X(\omega)}}{F_{X(\omega)}} \right] \right\| = \frac{\omega^2}{\left\{ \left(K_{S_X} - \omega^2 M_{S_X} \right)^2 + \left(\omega C_{S_X} \right)^2 \right\}^{1/2}} \qquad (2)$$

where ω denotes frequency. Figure 8 shows the amplitude of the recorded accelerance transfer function $\left| a_{X(\omega)} / F_{X(\omega)} \right|$ and the curve fit equation (2). The identified mass[9] M_{S_X} = 0.82 kg, support

[9] This is an effective mass adding the mass of the bearing (0.59 kg), the cage end disk (125.3 g) and the effective mass of the 8 rods.

stiffness K_{S_X} = 19.4 kN/m, and damping coefficient C_{S_X} = 9.5 Ns/m. The goodness of fit is R^2 = 0.966 in the frequency range to 150 Hz.

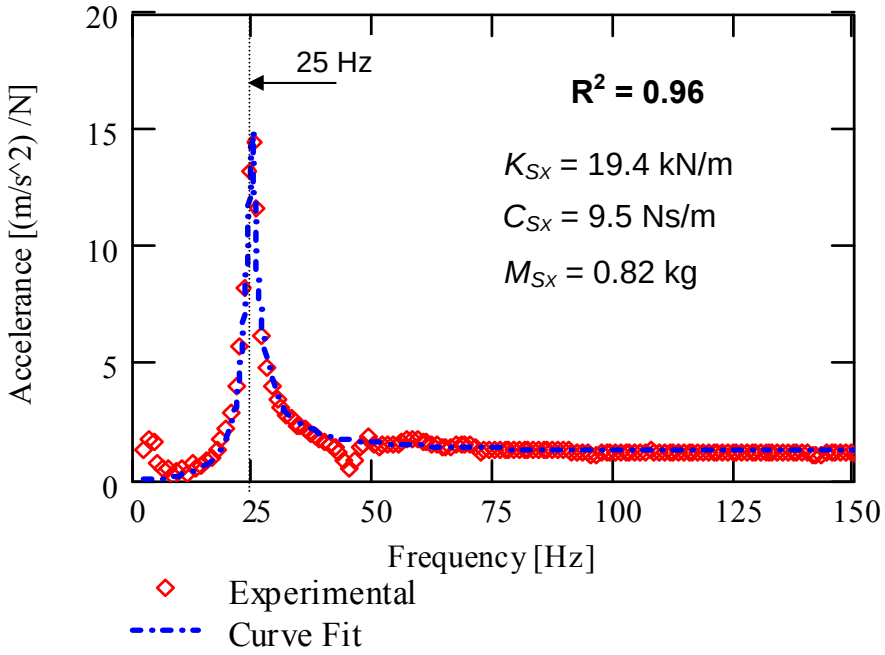

Fig. 8 Accelerance $|a_X/F_X|$ and curve fit to identify parameters of bearing elastic support structure

Similarly, Figure 9 displays the amplitude of the recorded accelerance transfer function $\left|a_{Y(\omega)}/F_{Y(\omega)}\right|$ and a curve fit identifying the elastic support coefficients along the Y direction: mass M_{S_Y} = 0.88 kg, K_{S_Y} = 21.2 kN/m, and C_{S_Y} = 6.6 Ns/m (ζ=0.024), with a goodness of fit of R^2 = 0.95 in the frequency range to 150 Hz.

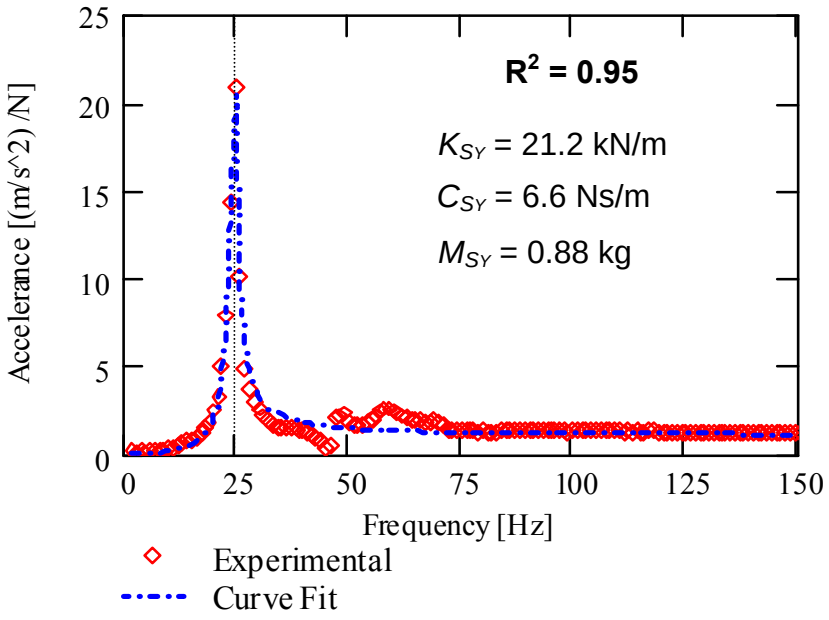

Fig. 9 Accelerance $|a_Y/F_Y|$ and curve fit to identify parameters of bearing elastic support structure

The identified bearing structure coefficients along X and Y directions, listed in Table 2, are nearly identical (within the experimental uncertainty), hence the support structure may be regarded as isotropic. The uncertainty in the identified parameters follows from the uncertainties in the load cell (1% linearity), accelerometer (1% linearity) and frequency resolution (1 Hz).

Table 2 Mechanical parameters for bearing and elastic support structure

	X direction	Y direction	
Stiffness, K_S	19.4±0.9	21.2±1.0	kN/m
Mass, M_S	0.81±0.02	0.88±0.02	kg
Damping, C_S	9.5±0.2	6.6±0.2	N.s/m
Natural frequency	24±1	24±1	Hz
Damping ratio, ζ	0.038	0.024	
R^2	0.96	0.95	

PARAMETER IDENTIFICATION PROCEDURE

The test rotor is balanced in place prior to conducting dynamic load measurements. The shop air supply drives the TC turbine to a constant rotor speed. Measurements hereby reported are conducted at a fixed shaft speed of 50 krpm (833 Hz)[10].

Bearing displacements synchronous with rotor speed are relatively small when compared to the forced displacements induced by the shaker loads. Note that the journal does also displace since the rotating shaft is not rigid; hence, it is important to make a distinction between bearing absolute displacements (X,Y) and those relative to the journal (x=X-X_J, y=Y-Y_J).

External (shaker) loads, F_X and F_Y, are exerted on the test bearing cartridge which displaces with absolute accelerations (a_X, a_Y), and displacements (x, y) relative to the journal. The equations of motion (EOM) for the bearing cartridge are

$$\begin{pmatrix} M_{S_X} a_X \\ M_{S_Y} a_Y \end{pmatrix} + \begin{pmatrix} C_{S_X} v_X \\ C_{S_Y} v_Y \end{pmatrix} + \begin{pmatrix} K_{S_X} X \\ K_{S_Y} Y \end{pmatrix} + \begin{bmatrix} C_{XX} & C_{XY} \\ C_{YX} & C_{YY} \end{bmatrix} \begin{pmatrix} \dot{x} \\ \dot{y} \end{pmatrix} + \begin{bmatrix} K_{XX} & K_{XY} \\ K_{YX} & K_{YY} \end{bmatrix} \begin{pmatrix} x \\ y \end{pmatrix} = \begin{pmatrix} F_X \\ F_Y \end{pmatrix} \tag{3}$$

where $\left(K_{ij}, C_{ij}\right)_{i,j=X,Y}$ are the test bearing stiffness and damping force coefficients. Note that $v_X = \dot{X}$ while $\dot{x} = {dx}/{dt} = v_X - \dot{X}_J$, for example.

The time domain force and motion are transformed into the frequency domain by applying the Discrete Fourier Transform (*DFT*). The applied forces, displacements, and accelerations become [7]

$$\begin{bmatrix} \overline{F}_{X(\omega)} \\ \overline{F}_{Y(\omega)} \end{bmatrix} = DFT \begin{bmatrix} F_{X(\omega)} \\ F_{Y(\omega)} \end{bmatrix}; \quad \begin{bmatrix} \overline{x}_{(\omega)} \\ \overline{y}_{(\omega)} \end{bmatrix} = DFT \begin{bmatrix} x_{(t)} \\ y_{(t)} \end{bmatrix}; \quad \begin{bmatrix} \overline{A}_{X_{(\omega)}} \\ \overline{A}_{Y_{(\omega)}} \end{bmatrix} = DFT \begin{bmatrix} a_{X_{(t)}} \\ a_{Y_{(t)}} \end{bmatrix} \tag{4}$$

where ω is a frequency. Note that the DFT of velocity (derivative of displacement with respect to time) is, for instance along X direction, defined as $DFT\left[\dot{x}_{(t)}\right] = j\,\omega\,\overline{x}_{(\omega)}$ where j=$\sqrt{-1}$ is the imaginary unit. Incidentally, also note that

[10] Dynamic load tests were also conducted without journal rotation and with same static load (contact operation). See later for a comparison of the identified force coefficients.

$$DFT\left[v_{X(t)}\right]=\frac{a_{X(\omega)}}{j\,\omega},\ DFT\left[X_{(t)}\right]=-\frac{a_{X(\omega)}}{\omega^2} \tag{5}$$

In the frequency domain, Eqn. (3) becomes

$$\begin{bmatrix} K_{XX}+j\omega C_{XX} & K_{XY}+j\omega C_{XY} \\ K_{YX}+j\omega C_{YX} & K_{YY}+j\omega C_{YY} \end{bmatrix}\begin{pmatrix} \bar{x}_{(\omega)} \\ \bar{y}_{(\omega)} \end{pmatrix}=\begin{pmatrix} \bar{F}_{X_{(\omega)}} \\ \bar{F}_{Y_{(\omega)}} \end{pmatrix}-\begin{pmatrix} M_{S_X}+C_{S_X}/j\omega-K_{S_X}/\omega^2 \\ M_{S_Y}+C_{S_Y}/j\omega-K_{S_Y}/\omega^2 \end{pmatrix}\begin{pmatrix} \bar{A}_{X_{(\omega)}} \\ \bar{A}_{Y_{(\omega)}} \end{pmatrix}=\begin{pmatrix} \bar{G}_{X_{(\omega)}} \\ \bar{G}_{Y_{(\omega)}} \end{pmatrix} \tag{6}$$

Or in compact form,

$$\begin{bmatrix} H_{XX} & H_{XY} \\ H_{YX} & H_{YY} \end{bmatrix}\begin{pmatrix} \bar{x}_{(\omega)} \\ \bar{y}_{(\omega)} \end{pmatrix}=\begin{pmatrix} \bar{G}_{X_{(\omega)}} \\ \bar{G}_{Y_{(\omega)}} \end{pmatrix}\begin{bmatrix} H_{xx} & H_{xy} \\ H_{yx} & H_{yy} \end{bmatrix}\begin{pmatrix} \bar{X}_{(\omega)} \\ \bar{Y}_{(\omega)} \end{pmatrix}=\begin{pmatrix} \bar{F}_{X_{(\omega)}}-M_{est}\bar{A}_{X_{(\omega)}} \\ \bar{F}_{Y_{(\omega)}}-M_{est}\bar{A}_{Y_{(\omega)}} \end{pmatrix} \tag{7}$$

where $\mathbf{H}_{(\omega_k)}=\left(\mathbf{K}+j\,\omega_k\,\mathbf{C}\right)$ is the matrix of bearing impedances at discrete frequencies ω_k. Two **linearly independent** forced excitations are required to identify the eight bearing force coefficients (four stiffnesses and four damping parameters). This is accomplished by sequentially exciting the system along the X and Y directions, i.e., by applying loads of the form $\mathbf{F}^X=\begin{pmatrix} F_X & 0 \end{pmatrix}^T$ and $\mathbf{F}^Y=\begin{pmatrix} 0 & F_Y \end{pmatrix}^T$. The combined algebraic equations for the two sets of excitations are written as

$$\begin{bmatrix} H_{XX} & H_{XY} \\ H_{YX} & H_{YY} \end{bmatrix}\begin{bmatrix} \bar{x}^X & \bar{x}^Y \\ \bar{y}^X & \bar{y}^Y \end{bmatrix}=\begin{pmatrix} \bar{G}_X^X & \bar{G}_X^Y \\ \bar{G}_Y^X & \bar{G}_Y^Y \end{pmatrix}\Rightarrow\mathbf{H}\bar{\mathbf{z}}=\bar{\mathbf{G}} \tag{8}$$

At each frequency ω_k, the bearing impedance coefficients are obtained from $\mathbf{H}_{(\omega_k)}=\bar{\mathbf{G}}_{(\omega_k)}\,\bar{\mathbf{z}}^{-1}_{(\omega_k)}$.

Random errors (noise) present in the impedance coefficients are minimized by averaging the impedances obtained from ten different tests. Note that random errors in the estimated impedance function reduce approximately by $\sqrt{N}$, where N= 10 is the number of tests, upon averaging [20]

$$\mathbf{H}=\left(1/10\right)\sum_{m=1}^{10}\mathbf{H}_m \tag{9}$$

EXPERIMENTAL PROCEDURE, RESULTS AND DISCUSSION

In the measurements, a static load *(W)*[11] ~ 22N pulls the bearing along the vertical direction, see Fig. 5. To identify the bearing force coefficients, two unidirectional load vectors $(F_X, 0)^T$ and $(0, F_Y)^T$ are applied by alternately delivering sine sweep force excitations along X and Y directions. Fig. 10 shows typical force excitations versus time.

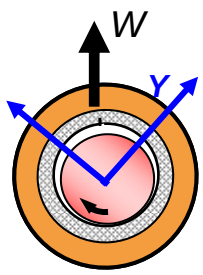

Preliminary tests showed that periodic loads with a fixed amplitude produced bearing displacements with amplitudes decreasing as the frequency increases. Since, the force coefficients of most bearings are nonlinear functions of the motion amplitudes (in particular if large relative to the bearing clearance), it is important to control the magnitude of the excitation force to maintain relatively constant bearing displacement amplitudes.

The formula for the construction of the sine-sweep load with excitation frequencies from 200 to 450 Hz, ensuring a fairly constant bearing displacement with respect to the journal, is

$$F_{(t)} = \left[F_o + (\Delta F)t\right] \sin\left[(\omega_o + \Delta\omega t)t\right] \qquad (10)$$

where F_o is the magnitude of the applied force at the initial frequency of ω_o, and ΔF and $\Delta\omega$ are the rate of increase in force and test frequency respectively. The rate of change in the magnitude of force (ΔF) and the test frequency ($\Delta\omega$) is determined based on the overall excitation time period and the desired final force and test frequency range. Figure 11 displays the average of ten excitation loads in the frequency domain. The selected frequency range [200 Hz-450 Hz] for the dynamic load measurements excludes a test system natural frequency at ~ 100 Hz. Unfortunately, no good record (data) evidencing the system resonance was kept.

[11] Recall the journal diameter D=38 mm and the bearing length L=38mm (L/D=1). Hence, the ratio W/LD=0.15 bar (2.21 psi) denotes the specific load pressure acting on the bearing.

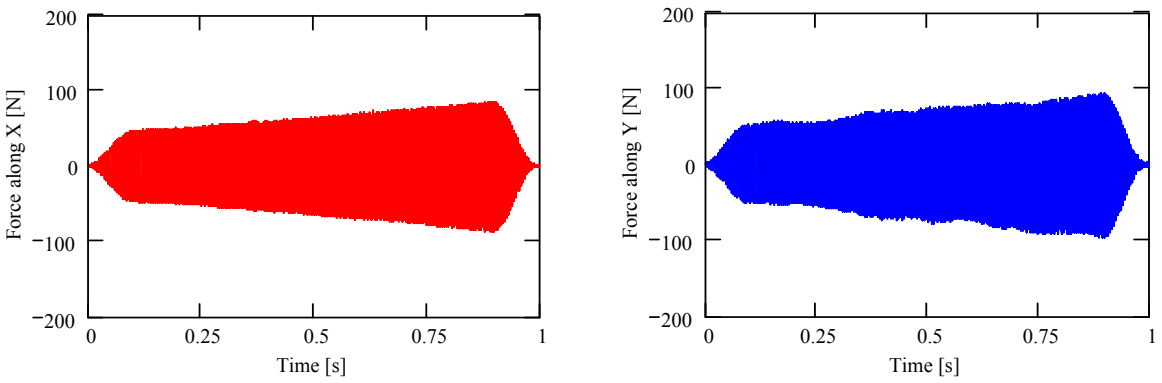

(a) *X*-direction load (b) *Y*-direction load

Fig. 10 Typical excitation forces along X and *Y* directions versus time. Multi frequency excitation (sine sweep 200-450 Hz)

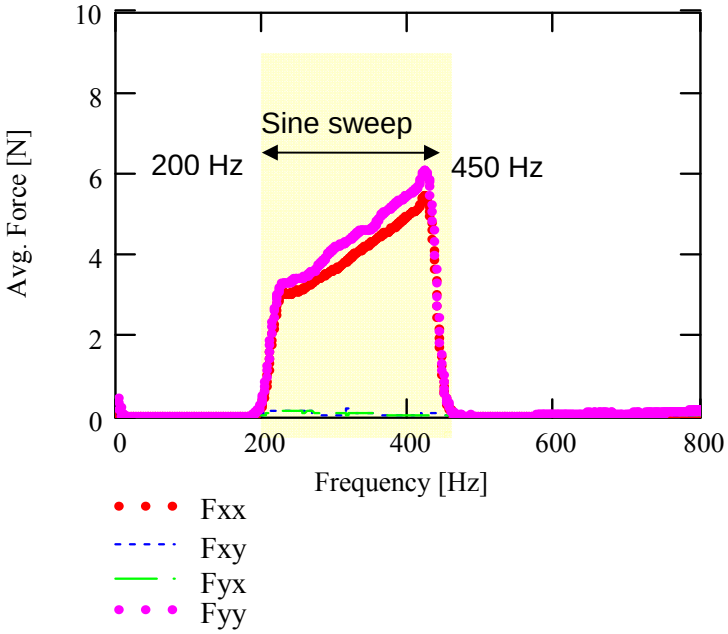

Fig. 11 *DFT* amplitude of excitation forces versus frequency. Average of 10 excitations

Figure 12 (left graph) shows the bearing relative displacement along the *X* direction due to an excitation force along the *X* direction. In the tests, the TC shaft spins at ~50 krpm (833 Hz). The graph on the right depicts the same displacements with all the frequencies above 500 Hz filtered. The filtered response removes any motions synchronous with the rotor angular frequency (833 Hz). Figure 13 likewise displays the other direct and cross directional bearing displacements due to the excitation loads. Recall that the recorded bearing motions are relative to the journal displacements.

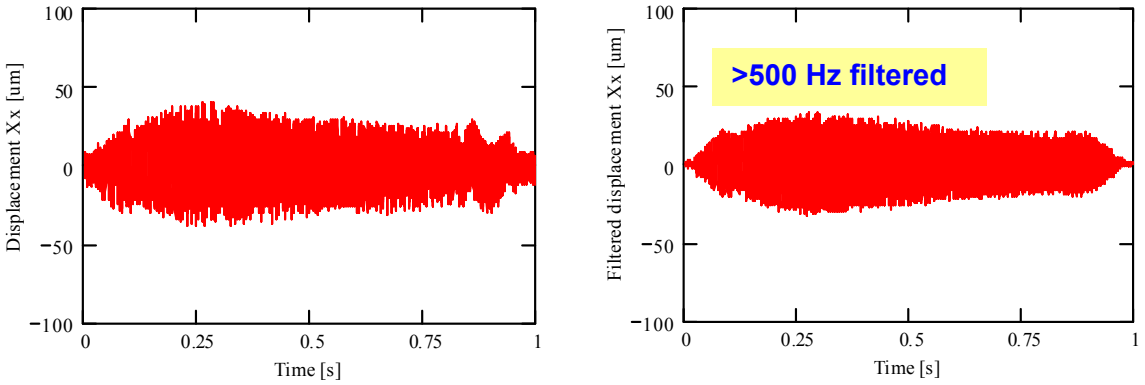

Fig. 12 Bearing relative displacement along *X* direction for shaker load along *X* direction. Rotor speed ~ 50 kprm (833 Hz). Motion amplitude ~ 30-40 μm. (Left) Unfiltered actual motions, (Right) motions with frequency >500 Hz filtered

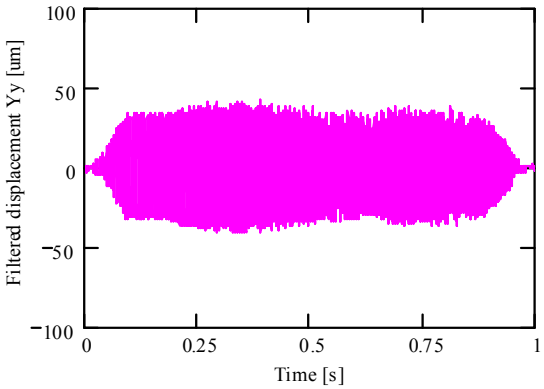

(a) *Y* bearing displacements due to load in *Y* direction

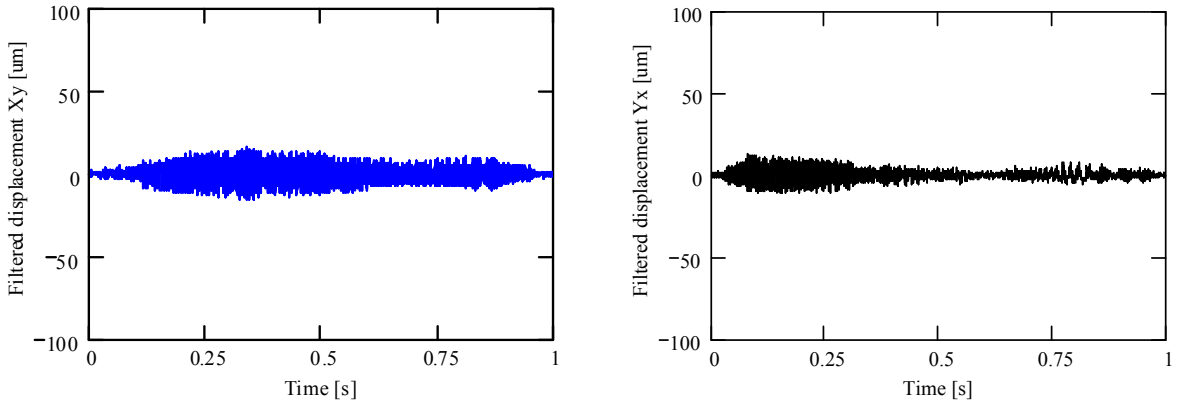

(b) *X* displacements due to load in *Y* direction (c) *Y* displacements due to load in *X* direction

Fig. 13 Filtered bearing relative displacement due to excitation forces. Rotor speed ~ 50 kprm (833 Hz). Controlled motion amplitude ~ 35- 45 μm. Filter cut-off frequency 500 Hz

Figure 14 displays the amplitude of the DFT for each of the bearing (relative) displacements versus frequency. The data represents averages from ten (consecutive) sine-sweep load excitations. Note that displacement components at the synchronous frequency are small relative to those within the excitation frequency range (200 Hz-450 Hz). Similarly, Figure 15 displays the DFT amplitude of the bearing accelerations.

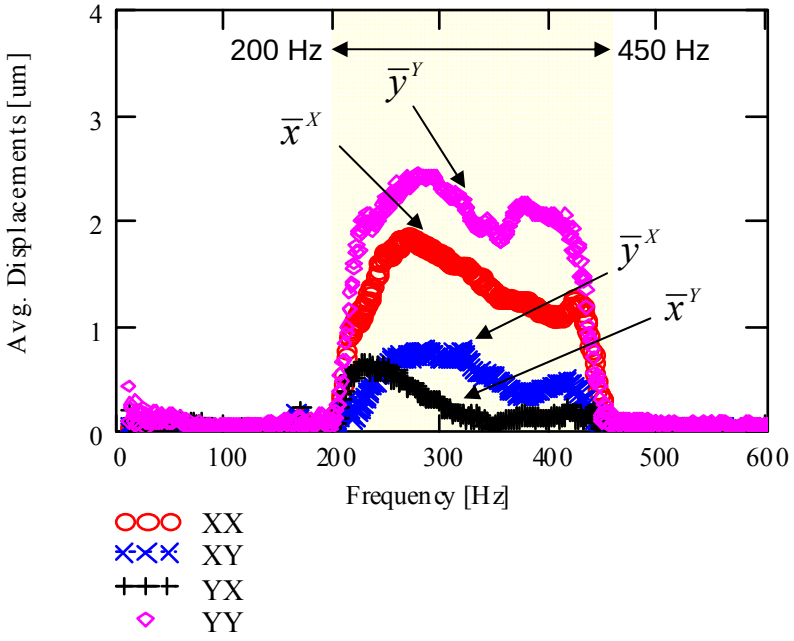

Fig. 14 *DFT* amplitude of bearing relative displacements (microns) versus excitation frequency. Average of 10 forced excitations. Rotor speed ~ 50 kprm (833 Hz)

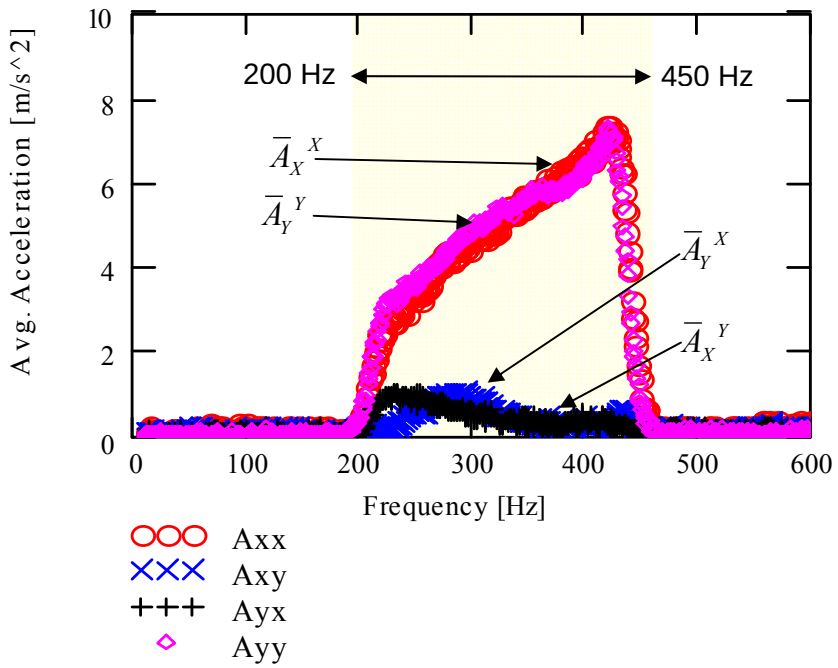

Fig. 15 *DFT* amplitude of bearing accelerations (m/s^2) versus excitation frequency. Average of 10 forced excitations. Rotor speed ~ 50 kprm (833 Hz)

ESTIMATED MMFB ROTORDYNAMIC FORCE COEFFICIENTS

Dynamic load measurements were conducted on the test MMFB without and with journal rotation[12] at 50 krpm (833 Hz), The identification procedure delivered the bearing stiffness $(K_{\alpha\beta})_{\alpha\beta=X,Y}$ and damping coefficients $(C_{\alpha\beta})_{\alpha\beta=X,Y}$ from the real and imaginary parts of the impedance functions, respectively, as functions of the excitation frequency (ω), i.e.,

$$\mathbf{K}_{(\omega_k)} = \mathrm{Re}\left(\mathbf{H}_{(\omega_k)}\right);\ \mathbf{C}_{(\omega_k)} = \frac{1}{j\omega_k}\,\mathrm{Ima}\left(\mathbf{H}_{(\omega_k)}\right) \qquad (11)$$

The measurements without journal rotation evidence the force coefficients of the metal mesh structure alone since there is no gas film separating the journal from its top foil. With journal rotation and since the bearing is airborne, i.e., with a minute gas film separating the spinning journal from the top foil (non contact operation); the force coefficients represent the combined (in series) action of the gas film and the metal mesh structure.

[12] At this rotational speed, the MMFB and shaft motions are stable, i.e. free of any sub harmonic whirl motions.

Stiffness coefficients Figure 16 shows the MMFB stiffness $(K_{\alpha\beta})_{\alpha\beta=X,Y}$ coefficients versus frequency. Without journal rotation, the cross-stiffnesses are negligible, $K_{XY} \sim K_{YX} \sim 0$; while $K_{XX} \sim K_{YY} \sim$ 0.3-0.4 MN/m , both relatively invariant with frequency. Note that prior experiments in a frequency range from [20-400 Hz] conducted with a thicker MMFB [1], as well as predictions based on an empirical model [4], show a bearing structural stiffness that raises (by as much as 70%) with increasing frequencies, as opposed to the current results in Fig.16(a) .

With shaft rotation at 833 Hz, the direct stiffnesses are nearly identical, $K_{XX} \sim K_{YY}$, in the frequency range 250-350 Hz[13], and similar in magnitude to the coefficients obtained without journal rotation. For higher frequencies, K_{XX} increases[14] while K_{YY} quickly drops to nil; the cause for the sudden reduction is unknown[15]. The cross stiffness coefficient K_{XY} is rather small; while K_{YX} shows an appreciable magnitude in the low frequency range (~ 300 Hz). Both cross coupled stiffnesses are practically nil in the upper end of the excitation frequency range. Recall that cross-coupled stiffnesses are due to gas film hydrodynamic shear effects and often are the culprits of rotordynamic instability.

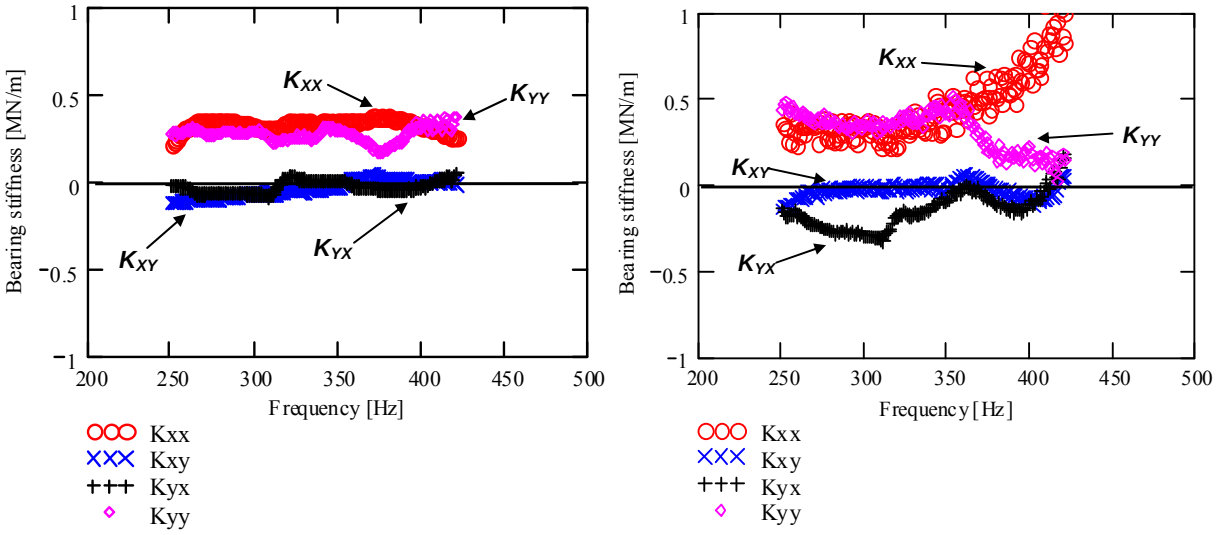

(a) without journal rotation (b) with journal rotation at 50 krpm (833 Hz).

Fig. 16 Identified MMFB direct (K_{XX}, K_{YY}) and cross coupled (K_{XY},K_{YX}) stiffnesses versus frequency. Journal speed: 0 and 50 krpm (833 Hz). Applied static load of 22 N (45° from *X* and *Y* axes)

[13] See Appendix A for a study on the repeatability of the force coefficients. Unfortunately, the present parameters are highly suspect (non repeatable) for excitation frequencies above 350 Hz.
[14] This is an expected result since gas films become stiffer as the excitation grows.
[15] A predictive model for metal mesh foil bearings is not available at this time.

As a side note, Ref. [3] reports impact load tests conducted on a thicker MMFB and the identification of rotordynamic force coefficients with the journal spinning at 50 krpm. The impacts excited motions with frequencies up to 200 Hz. The direct stiffnesses K_{XX}=K_{YY} are ~ 0.4 MN/m at 200 Hz, of the same order of magnitude as the current ones.

Damping coefficients Figure 17 shows the MMFB damping $(C_{\alpha\beta})_{\alpha\beta=X,Y}$ coefficients versus frequency. Without journal rotation, cross-damping coefficients are nil, $C_{YX} \sim C_{XY}$ =0 as expected; C_{YY} is nearly constant, while the direct damping coefficient C_{XX} decreases with excitation frequency. This is a typical result since the metal mesh structure offers material or hysteretic damping, best represented with a loss factor (γ). Hence, the equivalent viscous damping coefficient is $C \sim K\gamma/\omega$; that is, it decreases with frequency. Note that the magnitude of the metal mesh damping coefficients is rather high (600 to 200 Ns/m), thus making the test bearing system largely overdamped.

Recall that Ref. [1] shows bearing structure damping coefficients rapidly decreasing with frequency, from ~ 400 Ns/m at 200 Hz to ~100 Ns/m at 400 Hz. The current test results reveal damping coefficients that do not decay with increasing frequency.

For the measurements with journal rotation (833 Hz), the direct damping coefficients are similar, i.e., $C_{XX} \sim C_{YY}$ (~ 400 Ns/m), at low frequencies. Both direct coefficients show less frequency variation than the structural damping coefficients obtained without journal rotation. The cross coupled damping coefficients, $C_{XY} \sim -C_{YX}$, are but a small fraction of the direct damping coefficients. Prior estimation of the viscous damping coefficient in Refs. [1,3] shows a rapid decay with excitation frequency.

Incidentally, note that the MMFB direct force coefficients (stiffness and damping) are at least one order of magnitude larger than the bearing elastic support cage (see Table 2).

Appendix A shows the repeatability of the identified bearing rotordynamic force coefficients as determined from four sets of independent measurements. Thus far, force coefficients are consistent only over the low end of the excitation frequency span. For excitations above 350 Hz, the coefficients show great variability.

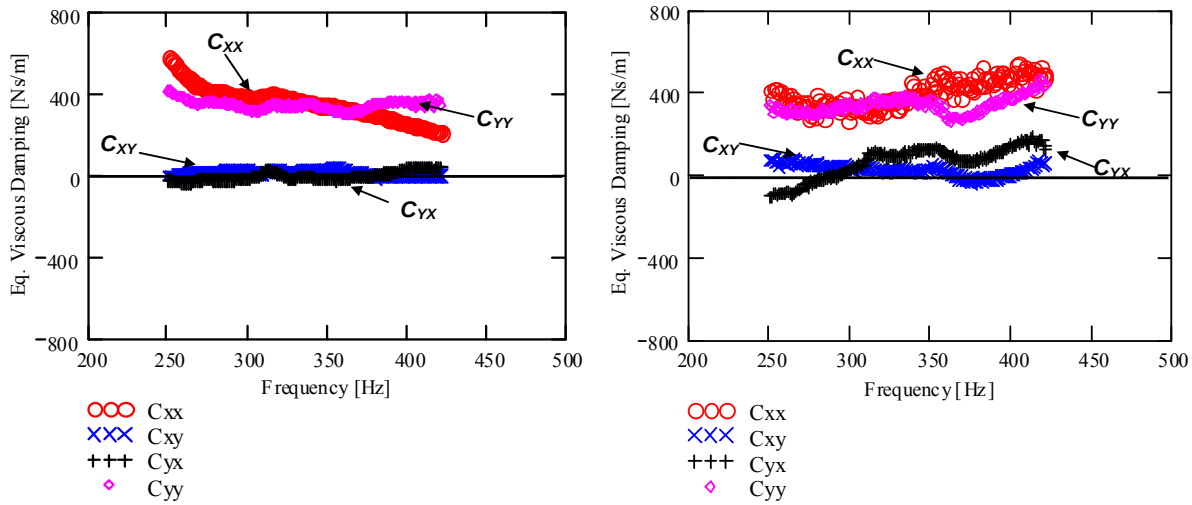

(a) without journal rotation (b) with journal rotation at 50 krpm (833 Hz).

Fig. 17 Identified MMFB direct (C_{XX}, C_{YY}) and cross coupled (C_{XY}, C_{YX}) damping coefficients versus frequency. Journal speed: 0 and 50 krpm (833 Hz). Applied static load of 22 N (45° from *X* and *Y* axes)

ESTIMATION OF MMFB LOSS FACTOR

Metal mesh bearings have an energy dissipation mechanism best described by material or hysteretic damping which is characterized by a loss factor (γ). This loss factor follows from a model that equates the energy dissipated by viscous damping (E_V) to the energy dissipated by material damping (E_M) over a full period of motion ($T = 2\pi / \omega$). Recall that for material damping

$$\mathbf{C} = \frac{\gamma}{\omega}\mathbf{K} \tag{12}$$

and from

$$E_v = \int_t^{t+T} \dot{\mathbf{z}}^{\mathrm{T}}\mathbf{C}\,\dot{\mathbf{z}}\,dt = E_M = \frac{\gamma}{\omega}\int_t^{t+T} \dot{\mathbf{z}}^{\mathrm{T}}\mathbf{K}\,\dot{\mathbf{z}}\,dt \tag{13}$$

it follows that

$$\gamma = \frac{\omega \int_t^{t+T} \dot{\mathbf{z}}^{\mathrm{T}}\mathbf{C}\,\dot{\mathbf{z}}\,dt}{\int_t^{t+T} \dot{\mathbf{z}}^{\mathrm{T}}\mathbf{K}\,\dot{\mathbf{z}}\,dt} \tag{14}$$

Clearly, the formulation above is path dependent, i.e., depends on the motion. The experiments were conducted with unidirectional sine-sweep loads that produced bearing motions $(x,y)_{(t)}$. In the absence of orthogonal motions, i.e., $(x \neq 0, y = 0)$ and $(x = 0, y \neq 0)$, it follows that $\gamma_x = \frac{\omega C_{XX}}{K_{XX}}$ and $\gamma_y = \frac{\omega C_{YY}}{K_{YY}}$ for periodic unidirectional motions along the *X*- and *Y*-directions only. However, two different loss factors is not a natural outcome.

For near circular orbits, Eq. (14) reduces to

$$\gamma = \frac{\omega\left(C_{XX}\left|V_X\right|^2 + C_{YY}\left|V_Y\right|^2\right)}{K_{XX}\left|V_X\right|^2 + K_{YY}\left|V_Y\right|^2} \tag{15}$$

where (V_X,V_Y) are the amplitudes of bearing velocity. For circular orbital motions, since $|V_X| = |V_Y|$, Eq. (15) reduces to

$$\gamma = \frac{\omega\left(C_{XX} + C_{YY}\right)}{K_{XX} + K_{YY}} \tag{16}$$

Figure 18 depicts the derived structural loss factor (γ) for the MMFB, derived from the test data shown in Figs. 17 and 18, and assuming circular orbit whirl motions. The analysis stops at 350 Hz because of the poor repeatability of the force coefficients above this frequency. Without journal rotation, the loss factor increases from 2 to 2.5 for frequencies ranging from 250 to 350 Hz. With journal rotation, γ increases from ~1.25 to 2.5 within the same frequency range. The large loss factors demonstrate the MMFB offers lots of viscous damping[16].

The current MMFB loss factor is much larger than that that identified for another MMFB [1], γ ~0.7, with a thicker metal mesh but of the same mesh density (20%). Ref. [3] using the same MMFB as in Ref. [1] gives γ ~0.5 derived from impact loads and with the journal spinning at 50 krpm. Further investigation is mandatory to assess the reason behind the apparently large loss factor for the MMFB with a thinner metal mesh ring.

[16] Elementary vibration analysis shows $\gamma = 2\zeta$, where ζ is a viscous damping ratio. Hence, $\zeta > 1$ denoting an overdamped system.

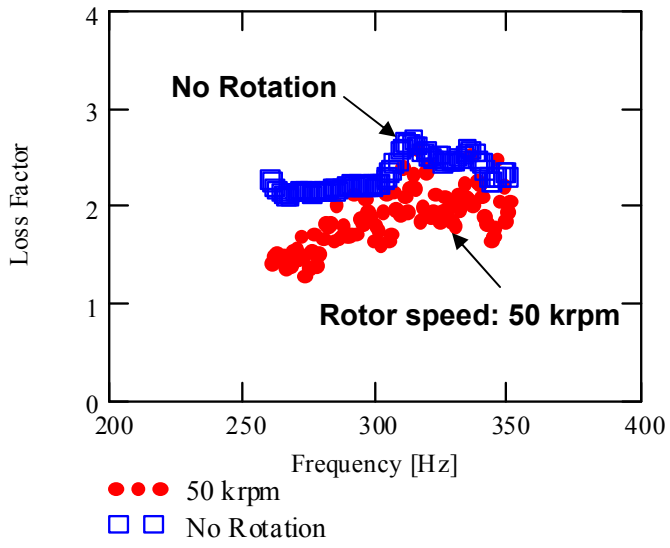

Fig. 18 Identified MMFB loss factor versus frequency. Journal speed: 0 and 50 krpm (833 Hz). Applied static load of 22 N (45° from *X* and *Y* axes)

UNEXPECTED FAILURE OF TOP FOIL

While operating the rotor at ~ 50 krpm, with static load of 22 N acting on the MMFB, the top foil temperature is ~ 40°C. The test TC driven rotor operated continuously for 2-3 hours per day over a stretch of 4-5 days while (repeated) the tests and measurements took place.

During later experiments, while the rotor turned at ~ 35 krpm (583 Hz), a sudden raise in the top foil temperature (~ 60°C) was recorded. Post-test inspection revealed marked wear, even loss of material, on the inboard end of the top foil. This type of damage is not unusual in bump-type foil bearings. **Appendix B** describes the damage and reasons that TC shaft elastic deformations can easily induce journal misalignment resulting in contact with the top foil inboard edge. Interestingly, the rest of the bearing and the rotor did not suffer permanent damage following the incident; hence the test system maintained its integrity.

CONCLUSIONS

Metal mesh foil bearings (MMFBs) have demonstrated reliable airborne operation and large energy dissipation ability [1-3], with material loss factors larger than those of commercially available bump-type foil bearings[17]. MMFBs quickly attenuate rotor vibrations due largely to the copper mesh material hysteresis. The MMFB technology is in its rudimentary stage, and requires experimental characterization of its rotordynamic behavior as a first step to compare with a forthcoming MMFB rotordynamic predictive tool, that couples an empirically developed metal mesh structural model and a hydrodynamic gas film model in series.

The report presents the identification of the rotordynamic force coefficients of a newly constructed MMFB, compact and robust in design with a thin metal mesh ring, suitable to replace commercially available GFB configurations. Orthogonally mounted electromagnetic shakers sequentially deliver controlled sine sweep load excitations (250-450 Hz), generating two linearly independent load vectors, and together with the recorded bearing accelerations and displacements relative to a journal render eight linearized force coefficients: four stiffness and four equivalent viscous damping coefficients. Multiple sets of independent tests demonstrate the identified force coefficients show too large variability for excitation frequencies greater than 350 Hz. Hence, the force coefficients are highly suspect of (yet) unknown errors.

With journal spinning at 50 krpm (833 Hz), the bearing direct stiffnesses, $K_{XX} \sim K_{YY}$, increase from 0.4 MN/m to 0.5 MN/m as frequency varies from 250 Hz to 350 Hz. At higher frequencies, K_{XX} increases while K_{YY} abruptly decreases. Cross coupled stiffness coefficients, K_{XY} and K_{YX}, are not significant with respect to the direct stiffnesses, except for K_{YX} at ~ 300 Hz. Without journal rotation, the bearing structural stiffnesses, K_{XX} and K_{YY}, are nearly identical and remain invariant with respect to frequency.

The identified equivalent viscous damping coefficients show the test bearing system is over damped. With no journal rotation, the bearing (structural) damping coefficient C_{XX} decreases from ~ 600 Ns/m to ~ 200 Ns/m, while C_{YY} remains at ~ 400 Ns/m. With journal rotation at 50 krpm, C_{XX} and C_{YY} gradually increase from 300 Ns/m to 500 Ns/m from 250 Hz to 420 Hz excitation frequency. The cross-damping coefficients, C_{XY} and C_{YX}, are small relative to the direct coefficients.

[17] There is abundant literature, in particular from TAMU, detailing static and dynamic load measurements to identify the material loss factor in bump-type foil bearings. To date, identified loss factors rarely exceed magnitudes > 0.5, more often γ~0.2–0.4, see Ref. [16] for example.

In general, the bearing force coefficients are less frequency dependent than prior measurements have shown [1, 3].

The test bearing shows a large magnitude material loss factor, γ>1, within the range of frequencies where the experimental force coefficients are reliable (250-350 Hz). Recall that a MMFB relies on structural damping for dissipation of mechanical energy. This loss factor is higher (γ>2) for the condition of no journal spinning. Bearing airborne operation at 50 krpm (83 Hz) reduces the loss factor, albeit increasing with frequency. Incidentally, the estimated loss factor values are surprisingly larger (at least two fold) in comparison with a similar MMFB, but with a thinner metal mesh ring, reported earlier [1,3].

Further experiments will continue, upon the construction of a new top foil to replace the existing damaged one, and characterize the MMFB rotordynamic force coefficients with varying motion amplitudes and rotor speeds. The MMFB displayed nonlinear structural characteristics in prior experiments [1, 3], and hence their proper characterization is of importance. Nonetheless, the MMFB clearly demonstrates its superior ability to dissipate energy and provide ample damping required for moderate load turbomachinery applications.

REFERENCES

[1] San Andrés, L., Chirathadam, T.A., and Kim, T.H., 2010, "Measurement of Structural Stiffness and Damping Coefficients in a Metal Mesh Foil Bearing," ASME J. Eng. Gas Turbines Power, **132**(3), p. 032503.

[2] San Andrés, L., Kim, T.H., Chirathadam, T.A., and Ryu, K., 2009, "Measurements of Drag Torque, Lift-Off Journal Speed and Temperature in a Metal Mesh Foil Bearing," *American Helicopter Society 65th Annual forum*, Grapevine, Texas, May 27-29.

[3] San Andrés, L., and Chirathadam, T. A., 2010, "Identification of Rotordynamic Force Coefficients of a Metal Mesh Foil Bearing using Impact Load Excitations," ASME Paper No. GT2010-22440.

[4] Choudhry, V., and Vance, J.M., 2005, "Design Equations for Wire Mesh Bearing Dampers in Turbomachinery," ASME Paper No. GT2005-68641.

[5] San Andrés, L., Kim, T.H., Ryu, K., Chirathadam, T. A., Jarrett, C., Hagen, K., Martinez, A., Rice, B., Niedbalski, N., Hung, W., and Johnson, M., " Gas Bearing Technology for Oil-Free Microturbomachinery – Research Experience for Undergraduate (REU) Program at Texas A&M University," ASME Paper No. GT2009-59920.

[6] Tiwari, R., Lees, A.W., and Friswell, M.I., 2004, "Identification of Dynamic Bearing Parameters: A Review," Shock and Vibrat. Digest, **36**, pp. 99-124.

[7] San Andrés, L., 2009, "Experimental Identification of Bearing Force Coefficients," Notes 14, Course on Modern LubricationTheory, Texas A&M University, http://rotorlab.tamu.edu/me626 [accessed on May 17, 2010]

[8] San Andrés, L., 1991, "Fluid Compressibility Effects on the Dynamic Response of Hydrostatic Journal Bearings," WEAR, Vol. 146, pp. 269-283.

[9] Rodriguez, L.E., and Childs, D.W., 2006, "Frequency Dependency of Measured and Predicted Rotordynamic Coefficients for a Load-on-Pad Flexible Pivot Tilting-Pad Bearing," ASME J.Tribol., **128**(2), pp. 388-396.

[10] Ku, C.-P. R., 1993, "An Experimental and Theoretical Study of the Dynamic Structural Stiffness in Compliant Foil Journal Bearings," *ASME 14th Biennial Conference on Mechanical Vibration and Noise*, Albuquerque, NM, DE-Vol. 63, ASME, New York, pp. 83–88.

[11] Kim, T.H., Breedlove, A.W., and San Andrés, L., 2009, "Characterization of Foil Bearing Structure for Increasing Shaft Temperatures: Part I-Static Load Performance," ASME J.Tribol., **131**(4), p.041703.

[12] Howard, S.A., 1999, "Preliminary Development of Characterization Methods for Compliant Air Bearings," Tribol. Transactions, **42** (4), pp. 789-794.

[13] Howard, S.A., DellaCorte, C., Valco, M.J., Prahl, J.M., and Heshmat, H., 2001, "Steady-State Stiffness of Foil Air Journal Bearings at Elevated Temperatures," Tribol. Transactions, **44**(3), pp. 489-493.

[14] Howard, S., DellaCorte C., Valco, M.J., Prahl, J.M., and Heshmat, H., 2001, "Dynamic Stiffness and Damping Characteristics of a High-Temperature Air Foil Journal Bearing," Tribol. Transactions, **44**(4), pp. 657-663.

[15] Lee, Y.-B., Park, D.–J., and Kim, C.–H., 2006, "Numerical Analysis for Bump Foil Journal Bearing Considering Top Foil Effect and Experimental Investigation," Paper-ID 229, *7th IFToMM-Conference on Rotor Dynamics*, Vienna, Austria.

[16] Kim, T.H., 2007, "Analysis of Side end Pressurized Bump Type Gas Foil Bearings: A Model Anchored to Test Data," PhD Dissertation, Texas A&M Univ. College Station, TX.

[17] Conlon, M.J., Dadouche, A., Dmochowski, W.M., Payette, R., Bedard, J.-P, and Liko, B., 2009, "Experimental Evaluation of Foil Bearing Performance: Steady-State and Dynamic Results," ASME Paper No. GT2009-60186.

[18] Glienicke, J., 1967, "Experimental Investigation of the Stiffness and Damping Coefficients of Turbine Bearings and their Application to Instability Prediction," Proc. Inst. Mech. Eng., **181**(3B), pp. 116-129.

[19] Childs, D., and Hale, K., 1994, "A Test Apparatus and Facility to Identify the Rotordynamic Coefficients of High-Speed Hydrostatic Bearings," J. Tribol., **116**, pp. 337-344.

[20] Rouvas, C., Murphy, B. T., and Hale, R.K., 1992, "Bearing Parameter Identification Using Power Spectral Density Methods," *Proc. of the Fifth International Conference of Vibrations in Rotating Machinery*, Bath, Englad, pp. 297-303.

[21] Carpino, M., Peng, J.P., and Medvetz, L., 1994, "Misalignment in a Complete Shell Gas Foil Journal Bearing," Tribol. Trans., **37**(4), PP. 829-835.

[22] Howard, S.A., 2009, "Misalignment in Gas Foil Journal Bearings: An Experimental Study," ASME J. Eng. Gas Turbines Power, **131**, pp.022501.

APPENDIX A: REPEATABILITY OF IDENTIFIED FORCE COEFFICIENTS

Four data sets of independent experiments were conducted and force coefficients identified to verify the repeatability of the measurements and the robustness of the identification procedure. A data set consists of ten independent X and Y dynamic load excitations. The operating conditions are 50 krpm in rotational speed and a vertical static pull load of 22 N.

Figures A.1 and A.2 depict the bearing stiffness and damping force coefficients for each dataset versus excitation frequency. The cross-stiffnesses (K_{XY}, K_{YX}) are nearly identical; however, the direct stiffnesses (K_{XX}, K_{YY}) show significant variability, in particular at the highest end of the excitation frequencies, > 350 Hz. Similarly, the cross damping coefficients (C_{XY}, C_{YX}) are nearly identical over the whole frequency range. As with the direct stiffnesses, direct damping coefficients (C_{XX}, C_{YY}) show different trends, in particular C_{XX}.

From 250 Hz to 300 Hz, the maximum variability in K_{XX}, K_{XY}, K_{YX}, and K_{YY} are 0.35 MN/m, 0.15 MN/m, 0.2 MN/m and 0.4 MN/m respectively; while for C_{XX}, C_{XY}, C_{YX}, and C_{YY} are 300 Ns/m, 75 Ns/m, 80 Ns/m and 150 Ns/m, respectively, Above 350 Hz, the variability for the direct coefficients is much larger; hence making the identified force coefficients suspect of error (not reliable).

Hence, it is apparent that repeatable and consistent force coefficients are identified within the low end of the excitation frequency range (< 350 Hz) only. Further efforts and procedural enhancements are urgently needed to improve the repeatability of the identified force coefficients.

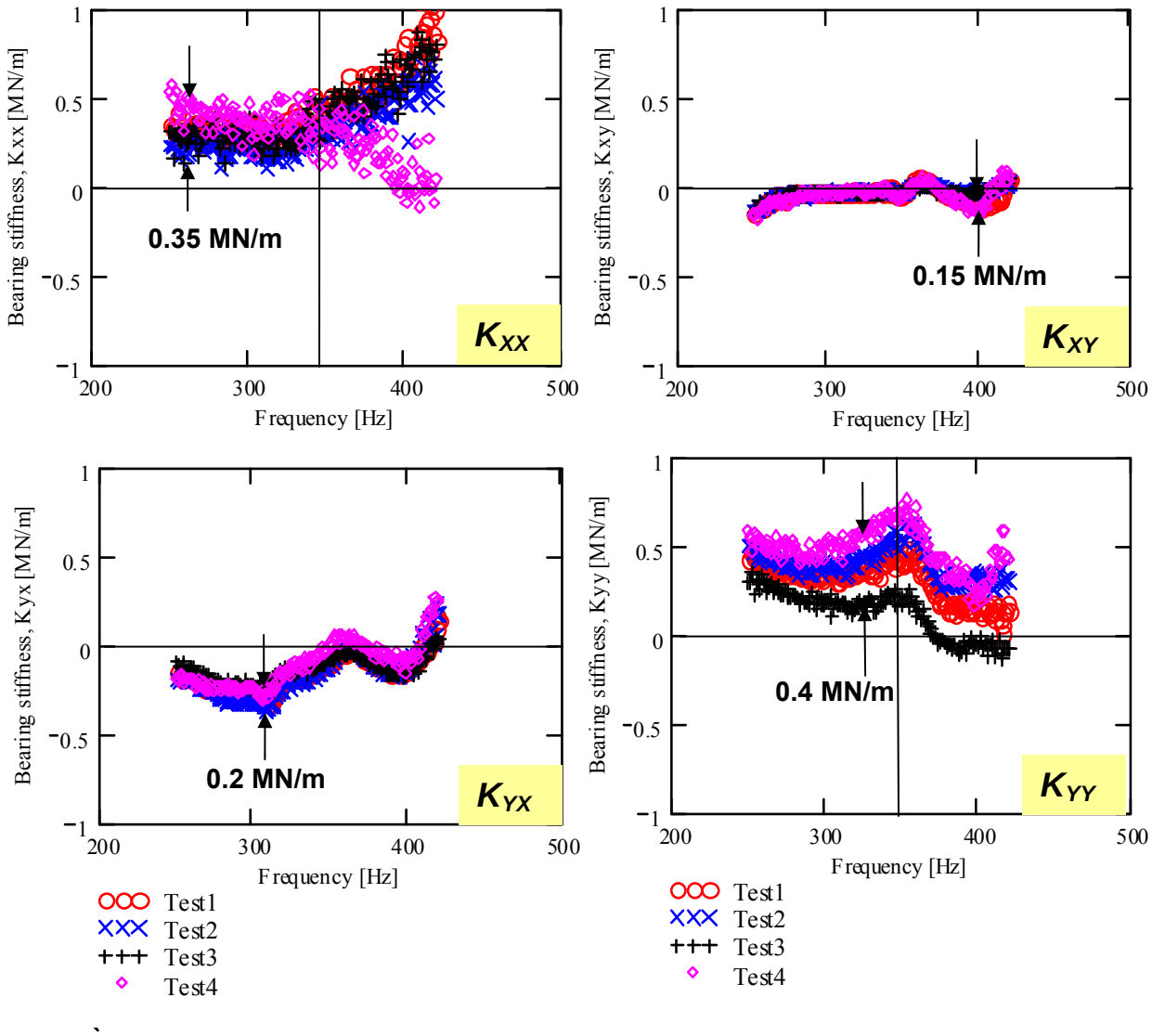

Fig. A.1 Test sets 1 – 4: Identified MMFB stiffness coefficients (K_{XX}, K_{YY}, K_{XY},K_{YX}) versus frequency. Journal speed =50 kprm (833 Hz). Applied static load of 22 N

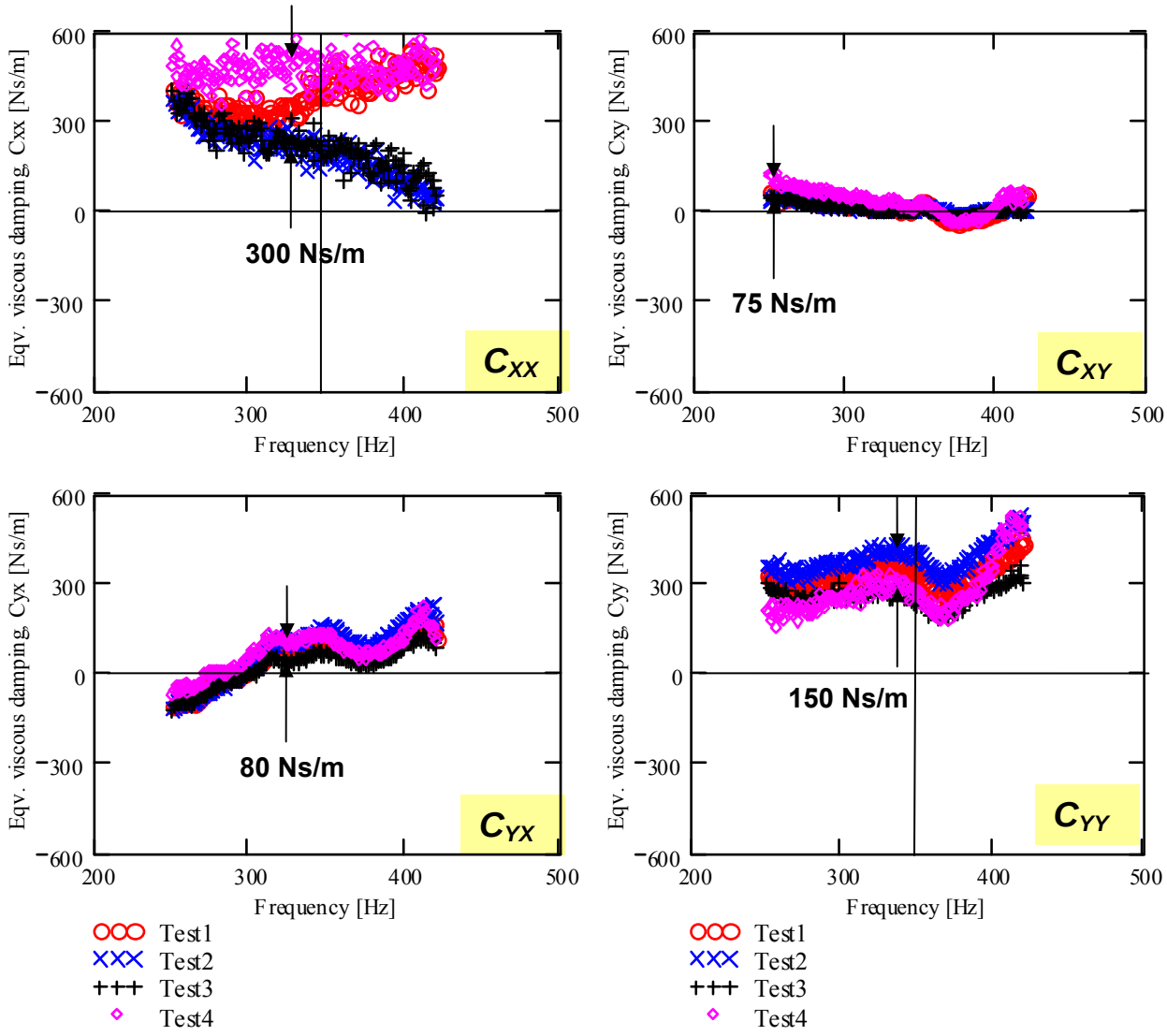

Fig. A. 2 Test sets 1-4: Identified MMFB damping coefficients (C_{XX}, C_{YY}, C_{XY}, C_{YX}) versus frequency. Journal speed = 50 kprm (833 Hz). Applied static load of 22 N

APPENDIX B. DAMAGE OF TOP FOIL

In a several hours continuous operation test, while the rotor turned at ~ 35 krpm and with an applied pull load of 27 N, the top foil outboard temperature suddenly rose to ~60°C; noticeable above the normal temperature of ~ 40 °C with the rotor spinning at 50 krpm. Hence, rubbing contact was suspected and rotor spinning was immediately halted. Note that the level of noise due to the TC turbine operation is far greater that that due to rubbing.

The bearing was removed from its journal. Inspection of the bearing revealed the top foil inboard edge had significant wear and loss of material. Figure B.1 depicts photographs of the (Inconel X-750) top foil in its pristine condition and after the experiments.) Inset shows the detail of the worn portion of the top foil.

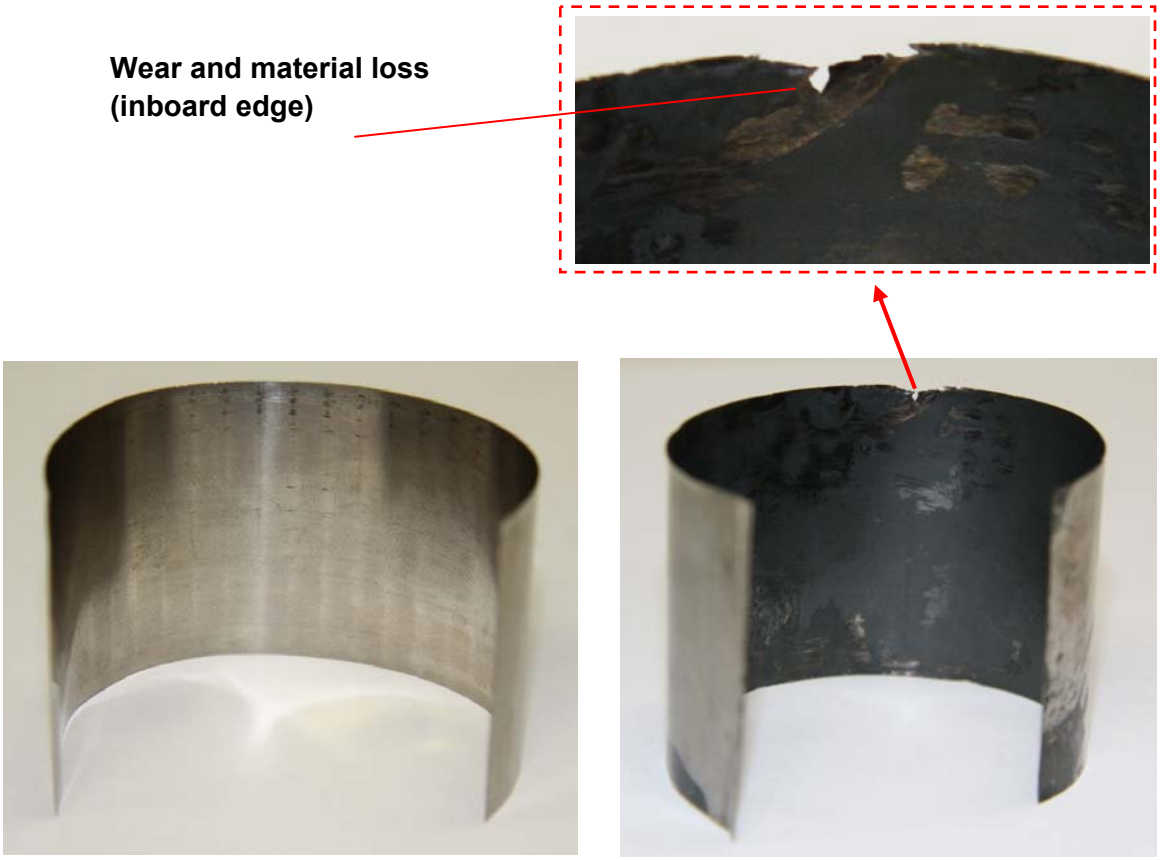

(a) Top foil before testing

(b) Top foil after failure
(Sprayed with MoS_2 < 5μm thick)

Fig. B.1 Photographs of top foil: original and after damage conditions

The top foil thickness is 0.12 mm and its original mass equals 4.58 g. Recall that prior to the experiments the top foil is spray-coated with a layer of MoS_2 (< 5 μm)The damaged foil mass is 4.546 g; hence, there is permanent loss of material (> 0.034 g) as is evident in the picture. The location of top foil material loss aligns with the vertical plane (see Fig. B.

Figure B.2 displays a photograph of the journal after the bearing was dismounted. Recall that the journal is spray-coated with 16 μm of Permalon®. This soft coating does not last too long, as prior experiments have demonstrated. Remains of the coating are visible on the inboard side. Note that the majority of the journal surface remains polished and free of wear marks. However, at the location of the foil inboard edge there is a 0.100 mm difference in diameter; the wear is likely due to rubbing contact with the top foil edge.

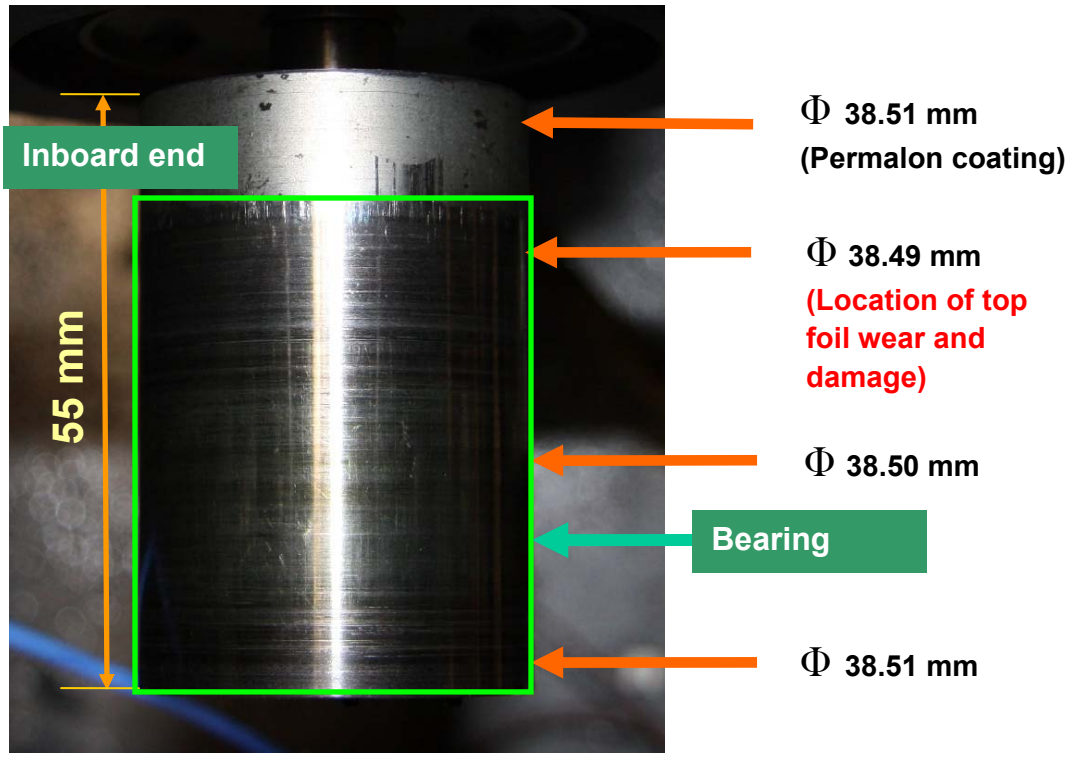

Fig. B.2 Photograph of journal, initially coated with Permalon®. Journal diameters along journal length noted

Suitable solid lubricant (coatings) are usually deposited on the top foil to reduce friction and delay wear during rotor startup and shutdown when rubbing contact between the journal and the top foil surface most likely occurs. During airborne operation, a gas hydrodynamic film lifts the rotor and eliminates the contact, hence the near friction free operation.

Foil bearings, after (many) hundreds of hours of continuous operation, show wear on the top foil axial sides (inboard and outboard) where the gas film hydrodynamic pressures are small (near ambient). The wear can be exacerbated by either pronounced rotor misalignment or by local shaft bending at the bearing edges. Predictive models [21] show GFB minimum film thickness decreasing with increasing misalignment. Smaller film thickness produce more heat generation as well [22].

Figure B.3 displays a schematic representation of the MMFB mounted on a test journal which is press fitted onto a shaft stub of a small turbocharger. The bearing displaces upwards as the static load is applied; and since the shaft is flexible, this same load deforms elastically the shaft. The journal is rigid and its displacement will be tilted with respect to the bearing; hence, contact between the two components likely occurs at the bearing inboard side, as depicted in the bottom graph.

Incidentally, note that the top foil material loss occurred over a very short span leaving a kink (sharp edges). Hence, it is also possible that wire mesh debris (or any other hard type) trapped while on assembly of the bearing on its journal could have quickly caused the damage.

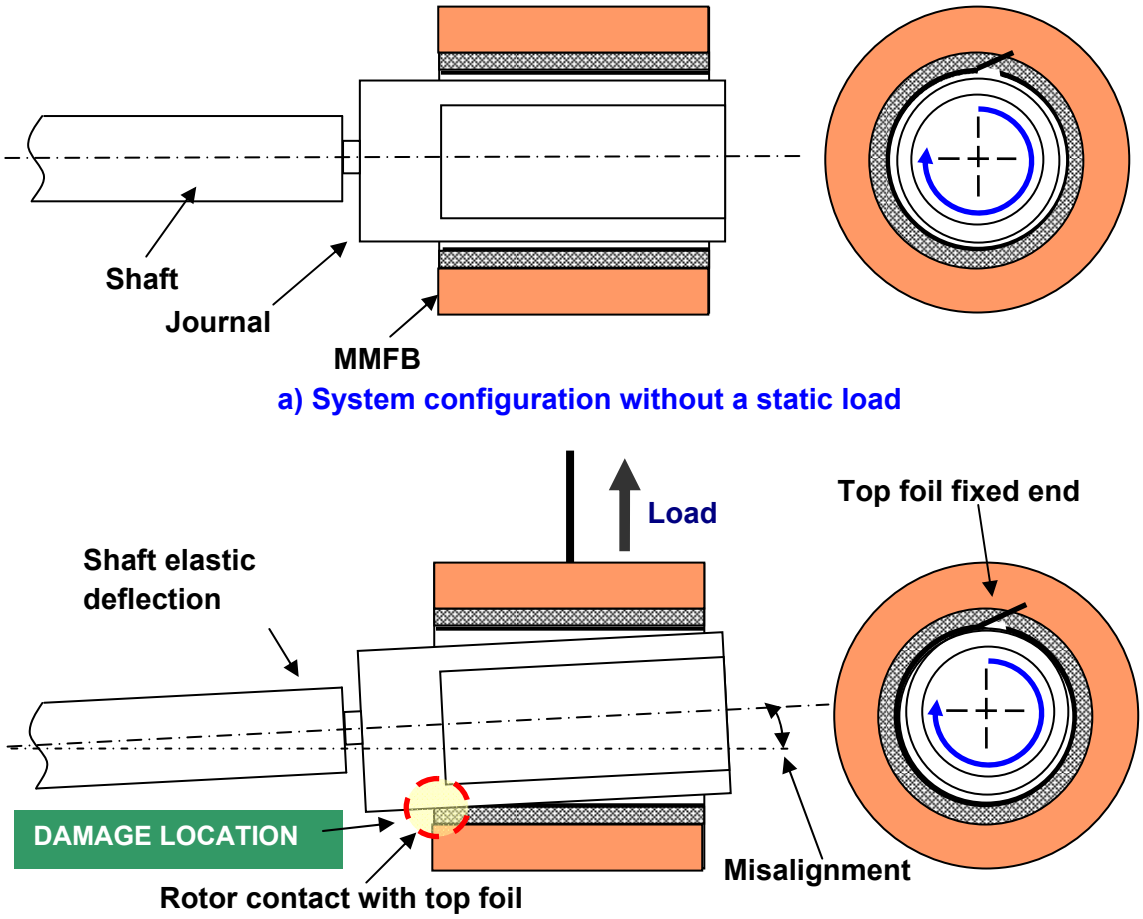

Fig. B.3 Schematic representation of displacements of MMFB and journal when acted by an external vertical load